nature medicine

LETTERS

https://doi.org/10.1038/s41591-019-0499-y

Inhibition of a G9a/DNMT network triggers immune-mediated bladder cancer regression

Cristina Segovia[1,2,3,14], Edurne San José-Enériz[2,4,14], Ester Munera-Maravilla[1,3,14], Mónica Martínez-Fernández[1,2,3,13], Leire Garate[2,5], Estíbaliz Miranda[2,4], Amaia Vilas-Zornoza[2,4], Iris Lodewijk[1], Carolina Rubio[2,3], Carmen Segrelles[1,2], Luis Vitores Valcárcel[2,4,6], Obdulia Rabal[7], Noelia Casares[8], Alejandra Bernardini[1,2], Cristian Suarez-Cabrera[3], Fernando F. López-Calderón[1,2,3], Puri Fortes[9], José A. Casado[10], Marta Dueñas[1,2,3], Felipe Villacampa[2,3], Juan José Lasarte[8], Félix Guerrero-Ramos[3,11], Guillermo de Velasco[3,12], Julen Oyarzabal[7], Daniel Castellano[1,2,12], Xabier Agirre[2,4*], Felipe Prósper[2,4,5*] and Jesús M. Paramio[1,2,3*]

Bladder cancer is lethal in its advanced, muscle-invasive phase with very limited therapeutic advances[1,2]. Recent molecular characterization has defined new (epi)genetic drivers and potential targets for bladder cancer[3,4]. The immune checkpoint inhibitors have shown remarkable efficacy but only in a limited fraction of bladder cancer patients[5–8]. Here, we show that high *G9a* (*EHMT2*) expression is associated with poor clinical outcome in bladder cancer and that targeting G9a/DNMT methyltransferase activity with a novel inhibitor (CM-272) induces apoptosis and immunogenic cell death. Using an immunocompetent quadruple-knockout (*Pten*$^{loxP/loxP}$; *Trp53*$^{loxP/loxP}$; *Rb1*$^{loxP/loxP}$; *Rbl1*$^{-/-}$) transgenic mouse model of aggressive metastatic, muscle-invasive bladder cancer, we demonstrate that CM-272 + cisplatin treatment results in statistically significant regression of established tumors and metastases. The antitumor effect is significantly improved when CM-272 is combined with anti-programmed cell death ligand 1, even in the absence of cisplatin. These effects are associated with an endogenous antitumor immune response and immunogenic cell death with the conversion of a cold immune tumor into a hot tumor. Finally, increased *G9a* expression was associated with resistance to programmed cell death protein 1 inhibition in a cohort of patients with bladder cancer. In summary, these findings support new and promising opportunities for the treatment of bladder cancer using a combination of epigenetic inhibitors and immune checkpoint blockade.

Bladder cancer (BC) is a heterogeneous disease that exhibits a wide spectrum of histological features, molecular alterations and subtypes[4]. Treatment of invasive tumors includes radical cystectomy and cisplatin (CDDP)-based chemotherapy[9]; the use of immune checkpoint inhibitors has been shown to increase survival, with responses in 20–30% of patients[5–8].

G9a, a histone methyltransferase that catalyzes H3K9 dimethylation, is altered in several human cancers[10] and has been proposed as an oncogene in BC[11]. Using The Cancer Genome Atlas (TCGA) database, we observed that in BC, *G9a* was primarily upregulated or amplified, mutations being very unusual (Extended Data Fig. 1a,b). Additionally, G9a-bound genes were downregulated in all BC molecular subtypes (Extended Data Fig. 1c), with significantly higher *G9a* RNA levels in basal/squamous tumors than in luminal tumors, and no differences according to tumor stage (Extended Data Fig. 1d–g).Using a series of non-muscle-invasive BC (NMIBC) patients[12,13] we observed significantly higher levels of *G9a* in tumor samples than in normal bladder tissue, in advanced-stage tumors, histological high-grade tumors and in recurrent or progressive tumors (Fig. 1a,b). High *G9a* messenger RNA and protein levels were associated with a statistically significant increase in BC recurrence (Fig. 1c and Extended data Fig. 1h,i). These results suggest that *G9a* overexpression in NMIBC is associated with poor clinical outcome and may represent a target in BC.

Next, treatment of different BC cell lines with a recently described dual G9a/DNMT inhibitor, CM-272 (ref. [14]), showed a potent inhibitory effect on cell proliferation, blocking cell cycle progression and inducing apoptosis and autophagy, which was associated with a decrease in H3K9me2 and 5-methylcytosine (Fig. 1d–h and Extended Data Fig. 2a). A combination of specific G9a (A-366 (ref. [15])) and DNMT (decitabine) inhibitors or the use of siRNA demonstrated a clear synergism of dual inhibition (Extended Data Fig. 2b–d). J82 and 253J BC cell lines, which were resistant to CM-272 treatment (Fig. 1d and Extended Data Fig. 2a), were characterized by *PIK3CA* mutations (Extended Data Fig. 2a)[16]. G9a interacts and

[1]Molecular Oncology Unit CIEMAT, Madrid, Spain. [2]Centro de Investigación Biomédica en Red Cáncer, Madrid, Spain. [3]Institute of Biomedical Research, University Hospital '12 de Octubre', Madrid, Spain. [4]Hemato-oncology Program, Centro de Investigación Médica Aplicada, IDISNA, Universidad de Navarra, Pamplona, Spain. [5]Hematology and Cell Therapy Department, Clínica Universidad de Navarra, Universidad de Navarra, Pamplona, Spain. [6]TECNUN, University of Navarra, San Sebastián, Spain. [7]Small Molecule Discovery Platform, Molecular Therapeutics Program, Centro de Investigación Médica Aplicada, Universidad de Navarra, Pamplona, Spain. [8]Immunology and Immunotherapy Program, Centro de Investigación Médica Aplicada, IDISNA, Universidad de Navarra, Pamplona, Spain. [9]Gene Therapy and Regulation of Gene Expression Program, Centro de Investigación Médica Aplicada, IDISNA, Universidad de Navarra, Pamplona, Spain. [10]Division of Hematopoietic Innovative Therapies (CIEMAT), Centro de Investigación Biomédica en Red de Enfermedades Raras and Advanced Therapies Unit, Instituto de Investigación Sanitaria Fundación Jiménez Díaz, Madrid, Spain. [11]Urology Department, University Hospital '12 de Octubre', Madrid, Spain. [12]Medical Oncology Department, University Hospital '12 de Octubre', Madrid, Spain. [13]Present address: Mobile Genomes and Disease Laboratory CIMUS, Universidad de Santiago de Compostela, La Coruña, Spain. [14]These authors contributed equally: Cristina Segovia, Edurne San José-Enériz, Ester Munera-Maravilla. *e-mail: xaguirre@unav.es; fprosper@unav.es; jesusm.paramio@ciemat.es

functionally cooperates with EZH2 in regulating H3K27me3; activating mutations in *PIK3CA* reduce EZH2 protein and H3K27me3 levels in BC[17], so resistance to CM-272 could be related to abnormal EZH2 activity. Indeed *PIK3CA*-mutated BC cells showed reduced EZH2 levels and increased protein kinase B (PKB/Akt) activity without changes in G9a (Fig. 1i). When the E545K *PIK3CA* mutant was expressed in sensitive RT112 cells, EZH2 and H3K27me3 were downregulated and cells became resistant to CM-272 (Fig. 1j). These results suggest a role for EZH2 in patients with BC[13,17] and indicate that certain mutations may represent a mechanism of resistance to CM-272.

Although CM-272 has no direct effect on EZH2 methyltransferase activity, we observed a decrease not only in H3K9me2 levels, but also in H3K27me3 (Fig. 1h). This finding is specific to BC since we have previously shown that CM-272 does not induce a decrease in H3K27me3 in hepatocarcinoma[18] or acute lymphoblastic leukemia[14]. Additional studies demonstrated that CM-272 did not inhibit wild-type or mutant variants of EZH2 (Extended Data Fig. 3a). G9a also primes the activity of EZH2 by catalyzing H3K27me1 (refs. [19,20]), so we ran time-course experiments and observed that a decrease in H3K9me2 and H3K27me1 levels preceded that of H3K27me3 (Fig. 1k). Overexpression or knockdown of *EZH2* conferred increased sensitivity or resistance, respectively, to CM-272 (Fig. 1l and Extended Data Fig. 3b). Collectively, these findings indicate the existence of a regulatory loop between G9a and EZH2 in BC with no direct effect of CM-272 on EZH2 methyltransferase activity. The positive correlation between *G9a* and *EZH2* (Extended Data Fig. 3c), and the fact that expression of transcripts cobound by G9a and EZH2 (ref. [20]) distinguish non-tumor samples from recurrent and non-recurrent tumors in an unsupervised manner (Fig. 1m), provide further support for the relationship between G9a and EZH2 in BC. Finally, we sought to demonstrate that although CM-272 efficacy in BC requires EZH2, the effect is not due to the methyltransferase activity of EZH2. Therefore, we analyzed the effect of combining an EZH2 inhibitor (GSK-126 (ref. [21])) with single inhibitors of G9a (A-366) or DNMT (decitabine) and found no synergism (Extended Data Fig. 3d–g). Collectively, these data indicate that CM-272 has a remarkable effect on BC cells, particularly in tumors without *PIK3CA* mutations.

We next examined the effect of CM-272 in combination with CDDP-based chemotherapy[22] in both in vitro and in vivo models of BC. CM-272 in combination with CDDP induced synergistic inhibition of proliferation of BC cells in vitro (Extended Data Fig. 4a). Similarly, in xenograft in vivo experiments, treatment with CM-272 (5 mg kg d^{-1}) and particularly with the CM-272 + CDDP combination, caused a significant decrease in tumor growth, increased apoptosis and autophagy and decreased H3K9me2 and H3K27me3 (Extended Data Fig. 4b–d).

To further examine the in vivo efficacy of CM-272, we used a newly developed quadruple-knockout (QKO) transgenic mouse model of metastatic BC, which is characterized by Cre-dependent inactivation of *Pten*, *Trp53* and *Rb1* tumor suppressor genes specifically in urothelial cells (AdK5Cre) of *Rbl1*-deficient mice[23,24]. Almost all mice developed invasive urothelial tumors and metastases in the lungs, liver and peritoneal cavity between 90–120 d after virus inoculation. At the early stage, tumors were characterized by extensive keratin 5 (K5) and p63 expression but reduced K20 expression (Fig. 2a,b), suggesting a basal/squamous type. Advanced-stage tumors and visceral metastases displayed reduced expression of K5 and p63, indicating a possible epithelial–mesenchymal transition program (Fig. 2a,b and Extended Data Fig. 5a). These findings were also supported by transcriptome analyses, indicating gene patterns similar to basal/squamous and opposite to luminal and luminal-papillary human BC subtypes (Extended Data Fig. 5b). Tumors and metastases were characterized by increased levels of G9a, Ezh2, H3K9me2 and H3K27me3, a complete absence of the targeted tumor suppressor genes and activation of ribosomal protein S6, PKB/Akt, extracellular signal-regulated kinase (Erk) and signal transducer and activator of transcription 3 (Stat3) (Fig. 2b–d). We analyzed whether the activation of these pathways and reduced *Pten* expression were associated with any specific group of human BC using the reverse phase protein array data present in the TCGA database. A self-organizing clustering of the human samples identified two clusters (named 6 and 9) that showed significant overlap, were enriched in basal/squamous, luminal-infiltrated and neuronal subtypes, were characterized by the simultaneous presence of *TP53* and *RB1* mutations, increased distant metastasis, increased *G9a* and *EZH2* expression and reduced patient survival (Extended Data Fig. 5c–i).

Treatment of QKO mice with CM-272 or with the CM-272 + CDDP combination produced a significant reduction in tumor and metastatic burden compared to the control group or the group treated with CDDP only (Fig. 2e,f). In most cases, animals treated with the CM-272 + CDDP combination only showed tumor remnants with

Fig. 1 | Relevance of *G9a* in human BC and effect of G9a/DNMT dual inhibitor in BC cells. a,**b**, *G9a* expression levels (RT–qPCR) in samples from a series of patients initially diagnosed with NMIBC, comparing normal versus primary tumors and their corresponding stages. $n = 87$ patient. **a**, Low- versus high-grade tumors, tumors that subsequently did or did not show recurrence and tumors that showed no progression versus tumors that did (**b**). *P* values were determined using a one-sided Mann–Whitney *U*-test. The relative expression value for each sample is shown along with mean ± s.e.m. for each group. Expression levels were normalized with respect to *TBP* expression. **c**, Kaplan–Meier graph showing tumor recurrence according to *G9a* mRNA levels (according to the median value) in human NMIBC samples. The *P* value was determined using a log-rank test. $n = 41$ independent patients (low *G9a* $n = 23$, high *G9a* $n = 18$ with regard to the median). **d**, GI_{50} values of CM-272 in BC cell lines. **e**, Cell cycle analysis in RT112 and 5637 cells after treatment with CM-272 (GI_{50} dose) analyzed by flow cytometry. Data are shown as the mean ± s.d. $n = 3$ independent experiments. The *P* value was estimated using a one-sided Mann–Whitney *U*-test. NS, not significant. **f**, Apoptosis was measured by FACS (annexin V) after treatment with CM-272 at different concentrations for 48 h. The data represent the mean ± s.d. $n = 3$ independent experiments. The *P* value was estimated using a one-sided Mann–Whitney *U*-test. **g**, Autophagy was measured by the expression of LC3B in 5637 cells after treatment with CM-272 (GI_{50}) at different time points using immunoblotting. **h**, H3K9me2 and H3K27me3 levels (immunoblotting) and 5-methylcytosine (dot blot) in RT112 cells after treatment with CM-272 (GI_{50}) at different time points. Total histone H3 was used to normalize loading. **i**, EZH2, AKT-P and G9a protein levels in different BC cell lines by western blotting. Actin was used to normalize loading. **j**, Proliferation of RT112 parental cells or RT112 cells transfected with the PIK3CA E545K construct after treatment with CM-272. Results represent the mean ± s.e.m. of $n = 3$ independent experiments (left panel). Protein expression of the cited proteins or histone marks in parental RT112 or mutated cells. Actin was used to normalize loading (right panel). **k**, Expression of EZH2, G9a, H3K9me2, H3K27me3 and H3K27me1 (immunoblotting) in RT112 cells after treatment with CM-272 (GI_{50}) at different time points. Tubulin and total histone H3 were used to normalize loading. **l**, Immunoblot showing the expression of the cited proteins or histone marks in parental RT112 cells or derivatives overexpressing (RT112 *EZH2*) or on knockdown of EZH2 (two different shRNA, shEZH2#1 and shEZH2#2, were used). Proliferation of RT112 cells or derivatives (overexpressing or knockdown for *EZH2*) after treatment with CM-272 is shown (right panel). Results represent the mean ± s.e.m. $n = 3$ independent experiments. **m**, Heatmap showing the unsupervised classification of NMIBC samples according to the expression levels of genes shown to be cobound by G9a and EZH2. **g–l**, A representative example of at least two independent experiments is shown. Full uncropped blots are available as Source data.

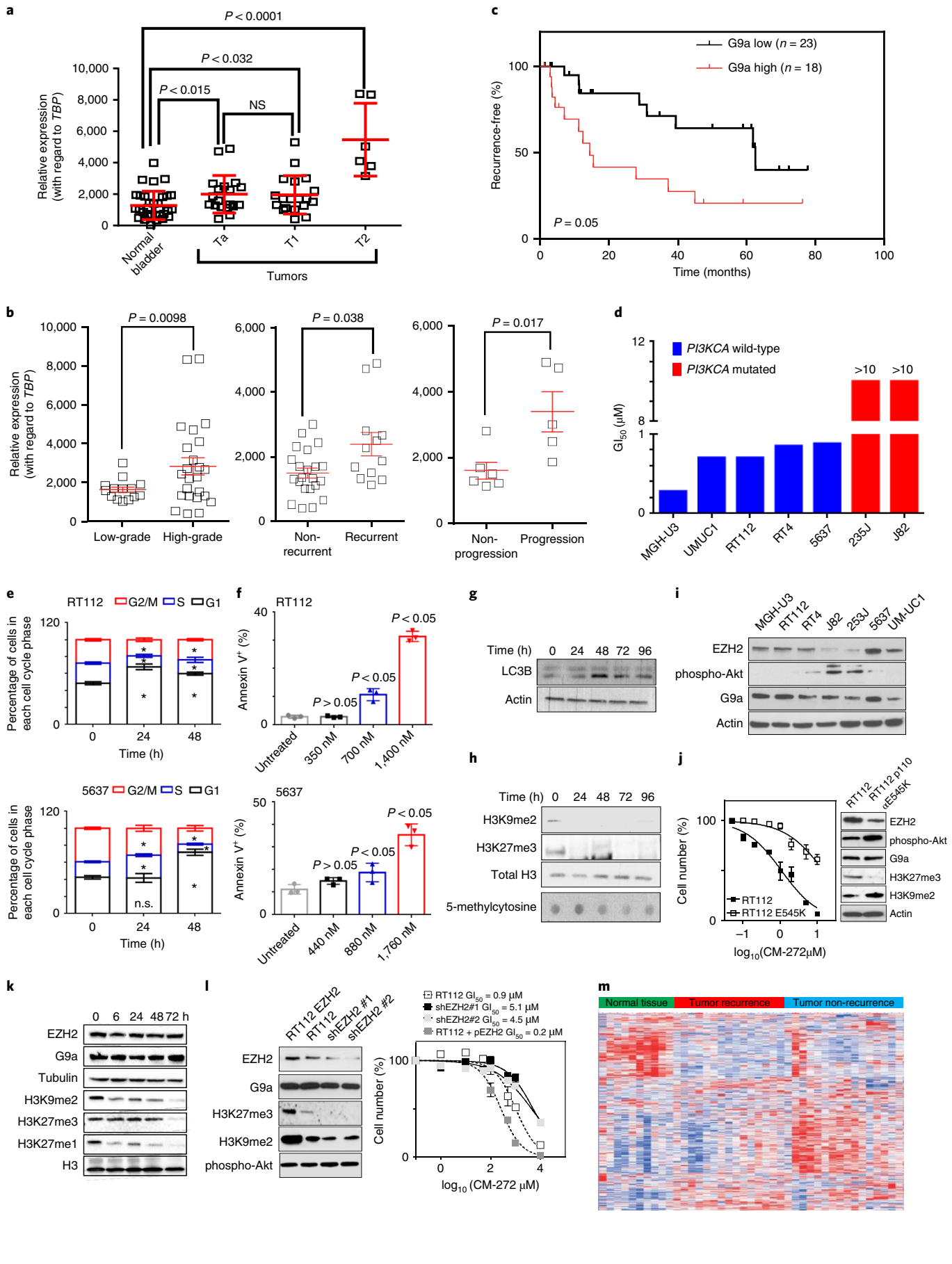
a
P < 0.0001
P < 0.032
P < 0.015
NS
Relative expression (with regard to TBP)
Normal bladder
Ta
T1
T2
Tumors
b
P = 0.0098
P = 0.038
P = 0.017
Low-grade
High-grade
Non-recurrent
Recurrent
Non-progression
Progression
c
G9a low (n = 23)
G9a high (n = 18)
Recurrence-free (%)
P = 0.05
Time (months)
d
PI3KCA wild-type
PI3KCA mutated
GI50 (μM)
>10
MGH-U3
UMUC1
RT112
RT4
5637
235J
J82
e
RT112 G2/M S G1
Percentage of cells in each cell cycle phase
Time (h)
5637 G2/M S G1
n.s.
f
RT112
Annexin V+ (%)
P < 0.05
P > 0.05
Untreated
350 nM
700 nM
1,400 nM
5637
440 nM
880 nM
1,760 nM
g
Time (h) 0 24 48 72 96
LC3B
Actin
h
H3K9me2
H3K27me3
Total H3
5-methylcytosine
i
MGH-U3
RT112
RT4
J82
253J
5637
UM-UC1
EZH2
phospho-Akt
G9a
Actin
j
Cell number (%)
RT112
RT112 E545K
log10(CM-272μM)
RT112 p110 αE545K
EZH2
phospho-Akt
G9a
H3K27me3
H3K9me2
Actin
k
0 6 24 48 72 h
EZH2
G9a
Tubulin
H3K9me2
H3K27me3
H3K27me1
H3
l
RT112 EZH2
RT112
shEZH2 #1
shEZH2 #2
EZH2
G9a
H3K27me3
H3K9me2
phospho-Akt
RT112 GI50 = 0.9 μM
shEZH2#1 GI50 = 5.1 μM
shEZH2#2 GI50 = 4.5 μM
RT112 + pEZH2 GI50 = 0.2 μM
Cell number (%)
log10 (CM-272 μM)
m
Normal tissue
Tumor recurrence
Tumor non-recurrence

reduced cell proliferation, increased apoptosis and autophagy, and decreased H3K9me2 and H3K27me3, without changes in *G9a* and *Ezh2* expression (Fig. 2d,g). We also observed that the tumors from animals treated with CM-272 + CDDP showed reduced enrichment of *E2f* and *Myc* target genes and genes involved in the epithelial–mesenchymal transition, clustering with normal bladder samples (Extended Data Fig. 5j,k and Supplementary Table 1). Moreover, gene set enrichment analysis (GSEA) revealed that treatment counteracted the gene repression mediated by the overexpression of *Ezh2* and reduced the expression of genes induced by *Egfr* (Extended Data Fig. 5l and Supplementary Table 2) without affecting S6, PKB/Akt, Erk and Stat3 activity (Fig. 2d).

To characterize the mechanism of action of CM-272 in BC, transcriptome analyses were performed in BC cell lines treated with CM-272 and in tumors from QKO mice treated with CM-272 + CDDP. In vitro, upregulation of genes implicated in immune response regulation with an enrichment in the interferon-α and -γ and tumor necrosis factor-α signaling pathways was observed, with a decrease in H3K9me2 in their promoter regions (Extended Data Fig. 6a–f and Supplementary Table 3). CM-272 treatment induced double-stranded RNA response, upregulation of several endogenous retroviruses[25] and significant increases in calreticulin expression and high mobility group protein B1 (HMGB1) secretion (Extended Data Fig. 6g–j), suggesting the presence of immunogenic cell death. We also observed increased expression of major histocompatibility genes; in the case of 5637 cells, this was accompanied by increased expression of the beta-2-microglobulin gene and natural killer cell ligands (Extended Data Fig. 6k,l). These results indicate a possible immune cell response.

Transcriptomic changes in vitro were mirrored by changes in vivo, with an increase in the expression of interferon-α and -γ, inflammatory response and allograft rejection genes, chemoattractants regulated by G9a and EZH2 and a decrease in various negative immunoregulatory cytokines after CM-272 + CDDP (Extended Data Fig. 7a,b and Supplementary Table 4). Positive interferon regulatory factors such as *Irf7* and *Irf8* were induced after treatment, while *Irf2*, which exerts a negative effect on Irf1-dependent transcription[26], was downregulated (Extended Data Fig. 7c). We found that various activators of T and natural killer (Extended data Fig. 7d,e) cell ligands and receptors were induced by the CM-272 + CDDP treatment in vivo. Finally, we observed a recovery of beta-2-microglobulin gene expression after treatment with CM-272 + CDDP (Extended Data Fig. 7f). Histologically, extensive infiltration of $CD8^+$ T and natural killer cells, together with a reduction in $CD163^+$ cells (Fig. 2h), was observed in treated tumors and metastases. Other immune cells, such as $FOXP3^+$ or $CD4^+$ cells, showed no significant changes after treatment (data not shown) suggesting an increase in the $CD8^+$/regulatory T cell ratio within the tumor after combined CM-272 + CDDP treatment. These results are consistent with recent studies, which demonstrated that epigenetic drugs may induce robust antitumor responses mediated by reducing cell proliferation and enhancing immune signaling[27–29]. Collectively these results suggest a conversion from non-inflamed 'cold' tumors to inflamed 'hot' tumors, more susceptible to respond to immune checkpoint inhibitors[30].

Next, QKO mice were treated with anti-programmed cell death 1 ligand 1 (PD-L1) alone or in combination with CM-272 or CM-272 + CDDP, based on the observation that PD-L1 was upregulated after in vitro treatment with CM-272 (Extended Data Fig. 8). Mice killed at mid-treatment (Fig. 3a) displayed similar incidences of tumors and metastases (Fig. 3b). However, groups treated with CM-272 + anti-PD-L1 showed extensive immune infiltrations composed of $CD3^+$, $CD8^+$ and natural killer cells with a very limited amount of $CD4^+$ and $CD163^+$ cells (Fig. 3c–l). At day 28, 75% of animals in the group treated with anti-PD-L1 alone showed evidence of tumors and metastases, while only 28 or 17% of the animals treated with CM-272 + anti-PD-L1, with or without CDDP, respectively, showed evidence of a primary tumor or metastatic disease (Fig. 3m–p). When mice treated with CM-272 + anti-PD-L1 (or CM-272 + CDDP + anti-PD-L1) were maintained for an additional 28 d without treatment, no significant tumor regrowth or metastases were observed (Fig. 3q). While remnants displayed clear signs of regression, small non-affected areas could be identified (Extended Data Fig. 9), suggesting that a single cycle of treatment could not completely eradicate every tumor in every mouse. Addition of CDDP to CM-272 + anti-PD-L1 was associated with renal toxicity. These data demonstrate that CM-272 not only increased the host immune reactivation against tumors and metastases, but also promoted a significant sustained response when combined with immune checkpoint blockade, providing a rationale for exploring this strategy in patients with BC.

Based on the fact that clinical responses to anti-PD-L1/programmed cell death protein 1 (PD-1) therapy occur more frequently in patients with inflamed tumors (reviewed in Chen and Mellman[31]), together with the results observed in our models and because only a limited fraction of patients with BC respond to immunotherapy[6], we decided to examine whether the expression and function of *G9a* and *EZH2* might be associated with responses to checkpoint inhibitors in BC. Using a cohort of CDDP-ineligible patients (two non-responders and one responder) with locally advanced and unresectable or metastatic urothelial cancer treated with anti-PD-1 as first-line therapy[32], we observed a significant increase in the levels

Fig. 2 | Combination of CM-272 and CDDP induces activation of immune-related pathways in a QKO transgenic model of BC. a, Double immunofluorescence staining showing the expression of K5 (green), K20 and p63 (Red) in early- and advanced-stage tumors. The insets denote the staining corresponding to the adjacent non-affected urothelium. The representative images of at least 6 independent samples obtained from 3–6 different animals are shown. **b**, Quantitative analysis of mRNA levels showing the relative expression of the keratin 5/keratin 20 ratio, the *G9a* and *EZH2* genes in normal bladder and mouse tumors. $n = 8$ animals (4 normal bladder and 4 mouse tumors). The results represent the mean ± s.e.m. The *P* value was estimated using a one-sided Mann–Whitney *U*-test. **c**, Immunohistochemistry images of early mouse tumors stained against the G9a (upper panel) and EZH2 proteins (lower panel). The representative images of at least 6 independent samples obtained from 3–6 different animals are shown. **d**, Immunoblot analyses of the cited proteins or histone marks in non-tumoral, untreated and treated bladder tumors from the transgenic mouse model. A representative example of two independent experiments is shown. Full uncropped blots are available as Source data. **e**, Kaplan–Meyer plot showing the tumor-free population in the transgenic mice cohorts (*n* as indicated for each group) at different time points with the indicated treatments. *P* values were determined using the log-rank test. **f**, Percentage of mice displaying overt or microscopic metastases in both cohorts. **g**, H&E-stained sections of untreated primary bladder tumors and immunohistochemistry images showing the reduction in proliferation (assessed by BrdU incorporation) in control versus treated mice. Induction of apoptosis (assessed by active caspase-3 staining) and autophagy (assessed by LC3B staining) in treated mice. H3K9me2 (control versus treated mice) and H3K27me3 (control versus treated mice) histone marks. The representative images of at least 6 independent samples obtained from 3–6 different animals are shown. Scale bars, 150 μm. **h**, Immunohistochemistry examples of untreated (vehicle) or CM-272 + CDDP-treated bladder tumors from transgenic mice showing an increase in $CD8^+$ T lymphocytes, massive infiltration of natural killer cells in the lesions and reduction in $CD163^+$ cells as a consequence of treatment. The representative images of at least 6 independent samples obtained from 3–6 different animals are shown. Scale bars, 150 μm.

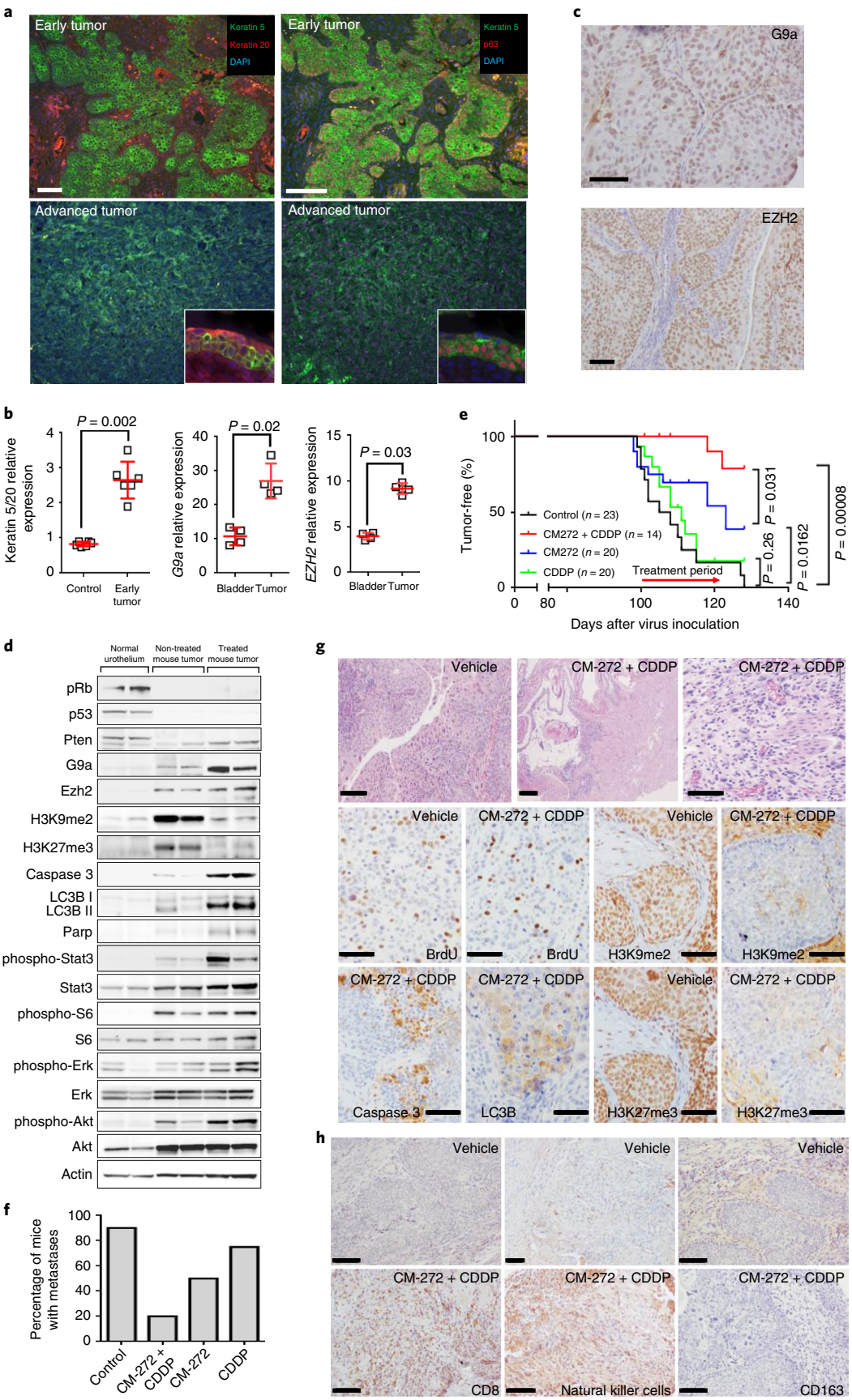
a
Early tumor
Keratin 5
Keratin 20
DAPI
Early tumor
Keratin 5
p63
DAPI
Advanced tumor
Advanced tumor
c
G9a
EZH2
b
P = 0.002
Keratin 5/20 relative expression
Control
Early tumor
P = 0.02
G9a relative expression
Bladder Tumor
P = 0.03
EZH2 relative expression
Bladder Tumor
e
Tumor-free (%)
Control (n = 23)
CM272 + CDDP (n = 14)
CM272 (n = 20)
CDDP (n = 20)
Treatment period
P = 0.031
P = 0.26
P = 0.0162
P = 0.00008
Days after virus inoculation
d
Normal urothelium
Non-treated mouse tumor
Treated mouse tumor
pRb
p53
Pten
G9a
Ezh2
H3K9me2
H3K27me3
Caspase 3
LC3B I
LC3B II
Parp
phospho-Stat3
Stat3
phospho-S6
S6
phospho-Erk
Erk
phospho-Akt
Akt
Actin
f
Percentage of mice with metastases
Control
CM-272 + CDDP
CM-272
CDDP
g
Vehicle
CM-272 + CDDP
CM-272 + CDDP
Vehicle
CM-272 + CDDP
Vehicle
CM-272 + CDDP
BrdU
BrdU
H3K9me2
H3K9me2
CM-272 + CDDP
CM-272 + CDDP
Vehicle
CM-272 + CDDP
Caspase 3
LC3B
H3K27me3
H3K27me3
h
Vehicle
Vehicle
Vehicle
CM-272 + CDDP
CM-272 + CDDP
CM-272 + CDDP
CD8
Natural killer cells
CD163

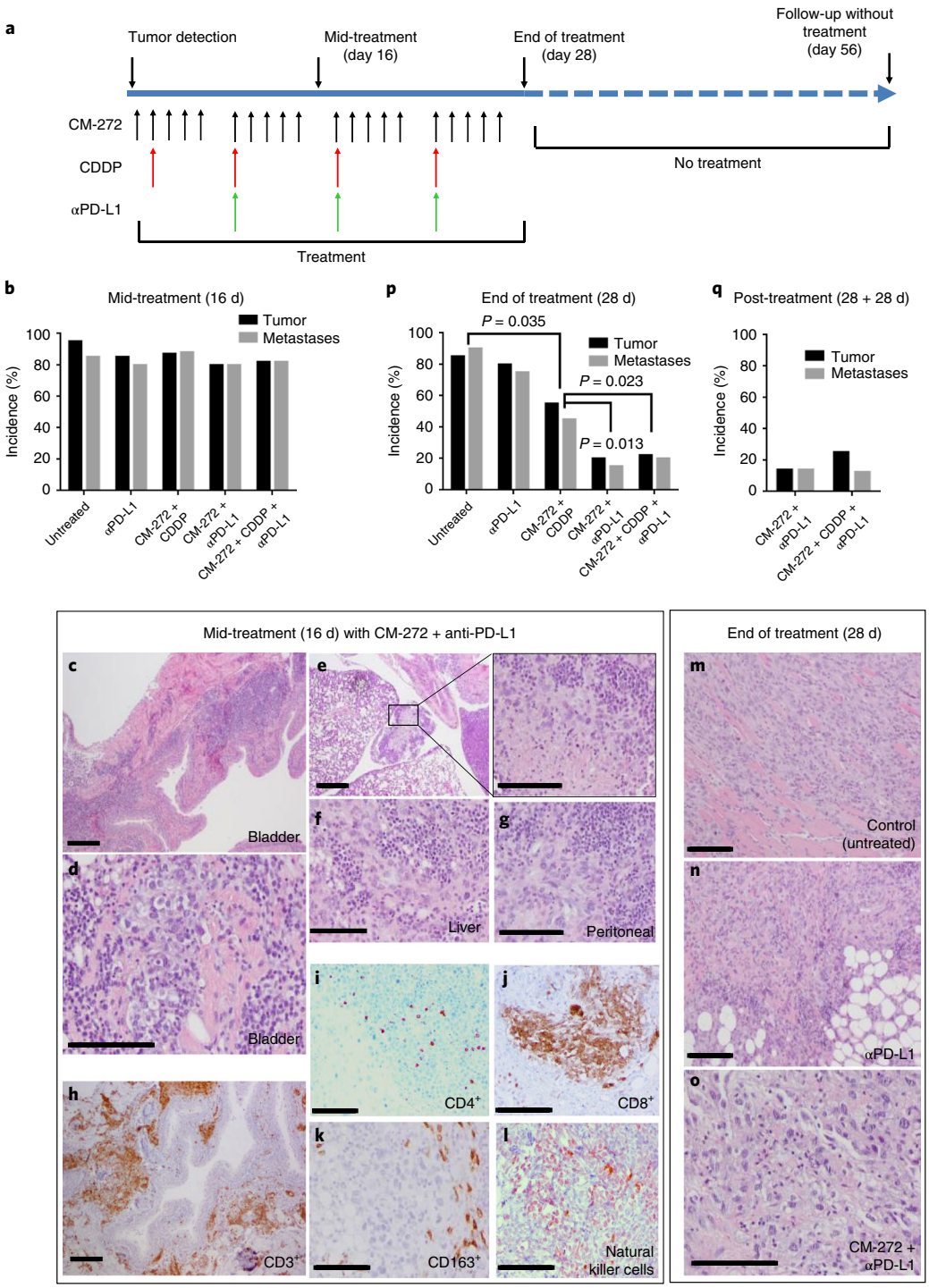

Fig. 3 | G9a/DNMT inhibition enhances responses to PD-L1 blockade and induces tumor regression. a, Schematic of the different protocols used to monitor the effect of the cited treatments in the QKO mouse model at different time points. The cohorts included untreated mice ($n=15$, killed at the mid-treatment time point (16 d, $n=9$) and at the end of treatment (day 28, $n=6$)), mice treated with anti-PD-L1 ($n=16$, killed at the mid-treatment time point (16 d, $n=8$) and at the end of treatment (day 28, $n=8$)), mice treated with CM-272 + CDDP ($n=20$, killed at the mid-treatment time point (16 d, $n=10$) and at the end of treatment (day 28, $n=10$)), mice treated with CM-272 + anti-PD-L1 ($n=21$, killed at the mid-treatment time point (16 d, $n=10$), at the end of treatment (day 28, $n=5$) and 28 d after the end of the treatment ($n=6$)) and mice treated with CM-272 + CDDP + anti-PD-L1 ($n=26$, killed at the mid-treatment time point (16 d, $n=7$), at the end of treatment (day 28, $n=11$) and 28 d after the end of the treatment ($n=8$)). **b**, Summary of tumor and metastasis incidence in the different cohorts of transgenic mice at the mid-treatment time point (16 d). **c**–**g**,**m**–**o**, H&E-stained images of tumors (**c**,**m**–**o**) and metastases (**e**–**g**) from untreated mice (**m**), mice treated with anti-PD-L1 (**n**) and mice treated with CM-272 + anti-PD-L1 (**c**–**f**,**o**) at the end of treatment (day 28) (**m**–**o**) or after 16 d of treatment (**c**–**g**). The representative images of at least four independent samples obtained from four different animals are shown. **h**–**l**, Immunohistochemistry showing the presence of $CD3^+$ (**h**), $CD4^+$ (**i**), $CD8^+$ (**j**), CD163+ (**k**) and natural killer cells (**l**) in mice after 16 d of treatment with CM-272 + anti-PD-L1. The representative images of at least four independent samples obtained from four different animals are shown. Scale bars, 150 μm. **p**, Summary of the incidence of tumors and metastases in the different cohorts of transgenic mice at the end of treatment (28 d). **q**, Post-treatment (28 d after the end of treatment). The *P* values in **p** were determined using the Fisher *F*-test, including all the animals from the different cohorts.

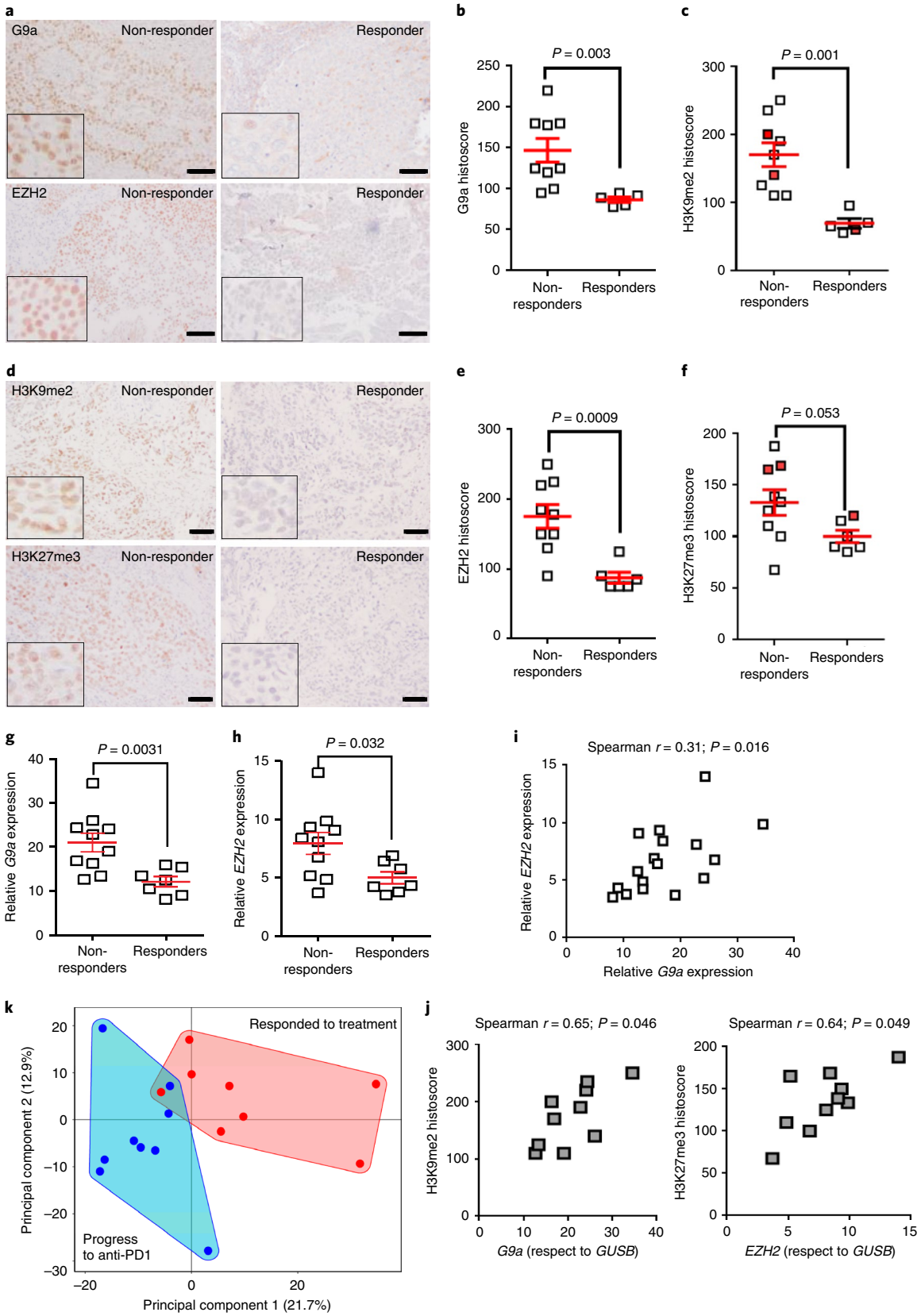

of *G9a*, *EZH2*, H3K9me2 and H3K27me3 in patients who did not respond to anti-PD-1 (Fig. 4a–h), which could not be explained by the presence of *KDM6A* mutations[33]. In addition, there was a positive correlation between *G9a*, *EZH2*, H3K9me2 and H3K27me3 (Fig. 4i,j); the gene signature corresponding to the *G9a* and *EZH2* cobound genes segregated advanced urothelial carcinoma patients who responded or progressed to anti-PD-1 first-line treatment (Fig. 4k and Extended Data Fig. 10). Finally, multivariate analysis

Fig. 4 | Levels of *G9a*, *EZH2*, H3K9me2 and H3K27me3 histone marks associated with clinical responses to anti-PD-1 immunotherapy in patients with BC. a, Representative immunohistochemistry images showing *G9a* and *EZH2* expression in primary tumor sections from CDDP-ineligible patients with locally advanced and unresectable or metastatic urothelial cancer showing non-response or response to anti-PD-1 immunotherapy as first-line therapy. Histological analyses and staining were performed in all clinical samples (patient), scoring 3–5 different sections from each tumor. Scale bars, 150 µm. **b**,**c**, Plot of the *G9a* (**b**) and H3K9me2 (**c**) histoscore in non-responders and responders to PD-1 blockade. The values for each tumor are shown as well as the mean ± s.d. for each group. The red squares in **c** identify patients bearing inactivating mutations in the *KDM6A* gene. $n = 9$ non-responder patients and $n = 5$ responder patients. The *P* value was estimated using a one-sided Mann–Whitney *U*-test. **d**, Representative immunohistochemistry images showing H3K9me2 and H3K27me3 levels in primary tumor sections from CDDP-ineligible patients with locally advanced and unresectable or metastatic urothelial cancer showing non-response or response to anti-PD-1 immunotherapy as first-line therapy. Histological analyses and staining were performed in all clinical samples (patient), scoring at least two different sections from of each tumor. Scale bars, 150 µm. **e**,**f**, Plots of EZH2 (**e**) and H3K27me3 (**f**) histoscore in non-responders and responders to PD-1 blockade. The value for each tumor sample is shown as well as the mean ± s.d. for each group. The red squares in **f** identify patients bearing inactivating mutations in the *KDM6A* gene. $n = 9$ non-responder patients and $n = 5$ responder patients. The *P* value was estimated using a one-sided Mann–Whitney *U*-test. **g**,**h**, Plot of mRNA expression of *G9a* (**g**) and *EZH2* (**h**) with regard to the *GUSB* gene in non-responders and responders to PD-1 blockade. The value for each tumor sample is shown as well as the mean ± s.d. for each group. $n = 10$ non-responder patients and $n = 7$ responder patients. The *P* value was estimated using a one-sided Mann–Whitney *U*-test. **i**,**j**, Correlation analysis between the expression of *G9a* and *EZH2* in all evaluable patient samples ($n = 17$ patients) (**i**), between *G9a* and H3K9me2 and between *EZH2* with H3K27me3 (**j**) in non-responders ($n = 10$ patient). **k**, Principal component analysis plot showing the differences regarding the *G9a* and *EZH2* cobound genes between advanced urothelial carcinoma patients that respond or progress to anti-PD-1 treatment. $n = 9$ responders to anti-PD-1 treatment; $n = 8$ non-responders to PD-1 treatment.

including various standard clinical-pathological parameters (sex, age, M (distant metastases) status, previous surgery of an NMIBC tumor, tumor location, number of cycles and toxicity) revealed that *G9a* expression was significantly associated with resistance to immunotherapy ($P = 0.011$), suggesting *G9a* as a potential biomarker for immune therapy in BC. Altogether, these data suggest a major role for chromatin remodeling in BC immunotherapy response, as previously indicated in other solid tumors[34,35].

In summary, our results provide a potentially new strategy to treat patients with BC based on the use of a previously unknown epigenetic inhibitor in combination with checkpoint inhibitors. Such provides potential biomarkers for response to immunotherapy; it also establishes the mechanisms of resistance to CM-272 based on the presence of *PIK3CA* mutations. To clinically explore a strategy based on the combination of epigenetic inhibitors targeting *G9a* together with the use of checkpoint inhibitors seems warranted to improve the response and quality of life of patients with BC and probably other types of human tumors.

Online content

Any methods, additional references, Nature Research reporting summaries, source data, statements of code and data availability and associated accession codes are available at https://doi.org/10.1038/s41591-019-0499-y.

Received: 15 June 2018; Accepted: 24 May 2019;
Published online: 03 July 2019

References

1. Zibelman, M. & Plimack, E. R. Systemic therapy for bladder cancer finally comes into a new age. *Future Oncol.* **12**, 2227–2242 (2016).
2. Sanli, O. et al. Bladder cancer. *Nat. Rev. Dis. Primers* **3**, 17022 (2017).
3. Weinstein, J. N. et al. Comprehensive molecular characterization of urothelial bladder carcinoma. *Nature* **507**, 315–322 (2014).
4. Robertson, A. G. et al. Comprehensive molecular characterization of muscle-invasive bladder cancer. *Cell* **171**, 540–556.e525 (2017).
5. Plimack, E. R. et al. Safety and activity of pembrolizumab in patients with locally advanced or metastatic urothelial cancer (KEYNOTE-012): a non-randomised, open-label, phase 1b study. *Lancet Oncol.* **18**, 212–220 (2017).
6. Bellmunt, J. et al. Pembrolizumab as second-line therapy for advanced urothelial carcinoma. *N. Engl. J. Med.* **376**, 1015–1026 (2017).
7. Balar, A. V. et al. Atezolizumab as first-line treatment in cisplatin-ineligible patients with locally advanced and metastatic urothelial carcinoma: a single-arm, multicentre, phase 2 trial. *Lancet* **389**, 67–76 (2017).
8. Rosenberg, J. E. et al. Atezolizumab in patients with locally advanced and metastatic urothelial carcinoma who have progressed following treatment with platinum-based chemotherapy: a single-arm, multicentre, phase 2 trial. *Lancet* **387**, 1909–1920 (2016).
9. Stenzl, A. et al. Treatment of muscle-invasive and metastatic bladder cancer: update of the EAU guidelines. *Eur. Urol.* **59**, 1009–1018 (2011).
10. Casciello, F., Windloch, K., Gannon, F. & Lee, J. S. Functional role of G9a histone methyltransferase in cancer. *Front. Immunol.* **6**, 487 (2015).
11. Li, F. et al. G9a inhibition induces autophagic cell death via AMPK/mTOR pathway in bladder transitional cell carcinoma. *PLoS ONE* **10**, e0138390 (2015).
12. Dueñas, M. et al. *PIK3CA* gene alterations in bladder cancer are frequent and associate with reduced recurrence in non-muscle invasive tumors. *Mol. Carcinog.* **54**, 566–576 (2015).
13. Santos, M. et al. In vivo disruption of an Rb-E2F-Ezh2 signaling loop causes bladder cancer. *Cancer Res.* **74**, 6565–6577 (2014).
14. San José-Enériz, E. et al. Discovery of first-in-class reversible dual small molecule inhibitors against G9a and DNMTs in hematological malignancies. *Nat. Commun.* **8**, 15424 (2017).
15. Sweis, R. F. et al. Discovery and development of potent and selective inhibitors of histone methyltransferase G9a. *ACS Med. Chem. Lett.* **5**, 205–209 (2014).
16. Earl, J. et al. The UBC-40 Urothelial Bladder Cancer cell line index: a genomic resource for functional studies. *BMC Genomics* **16**, 403 (2015).
17. Segovia, C. et al. Opposing roles of *PIK3CA* gene alterations to EZH2 signaling in non-muscle invasive bladder cancer. *Oncotarget* **8**, 10531–10542 (2017).
18. Bárcena-Varela, M. et al. Dual targeting of histone methyltransferase G9a and DNA-methyltransferase 1 for the treatment of experimental hepatocellular carcinoma. *Hepatology* **69**, 587–603 (2019).
19. Coward, W. R. et al. Interplay between EZH2 and G9a regulates *CXCL10* gene repression in idiopathic pulmonary fibrosis. *Am. J. Respir. Cell Mol. Biol.* **58**, 449–460 (2018).
20. Mozzetta, C. et al. The histone H3 lysine 9 methyltransferases G9a and GLP regulate polycomb repressive complex 2-mediated gene silencing. *Mol. Cell* **53**, 277–289 (2014).
21. McCabe, M. T. et al. EZH2 inhibition as a therapeutic strategy for lymphoma with EZH2-activating mutations. *Nature* **492**, 108–112 (2012).
22. Witjes, J. A. et al. EAU guidelines on muscle-invasive and metastatic bladder cancer: summary of the 2013 guidelines. *Eur. Urol.* **65**, 778–792 (2014).
23. Puzio-Kuter, A. M. et al. Inactivation of *p53* and *Pten* promotes invasive bladder cancer. *Genes Dev.* **23**, 675–680 (2009).
24. Rubio, C. et al. CDK4/6 inhibitor as a novel therapeutic approach for advanced bladder cancer independently of *RB1* status. *Clin. Cancer Res.* **25**, 390–402 (2019).
25. Chiappinelli, K. B. et al. Inhibiting DNA methylation causes an interferon response in cancer via dsRNA including endogenous retroviruses. *Cell* **162**, 974–986 (2015).
26. Wang, Y. et al. Negative feedback regulation of IFN-γ pathway by IFN regulatory factor 2 in esophageal cancers. *Cancer Res.* **68**, 1136–1143 (2008).
27. Stone, M. L. et al. Epigenetic therapy activates type I interferon signaling in murine ovarian cancer to reduce immunosuppression and tumor burden. *Proc. Natl Acad. Sci. USA* **114**, E10981–E10990 (2017).
28. Cribbs, A. et al. Inhibition of histone H3K27 demethylases selectively modulates inflammatory phenotypes of natural killer cells. *J. Biol. Chem.* **293**, 2422–2437 (2018).
29. Topper, M. J. et al. Epigenetic therapy ties MYC depletion to reversing immune evasion and treating lung cancer. *Cell* **171**, 1284–1300.e21 (2017).

30. Sharma, P. & Allison, J. P. The future of immune checkpoint therapy. *Science* **348**, 56–61 (2015).
31. Chen, D. S. & Mellman, I. Elements of cancer immunity and the cancer-immune set point. *Nature* **541**, 321–330 (2017).
32. Balar, A. V. et al. First-line pembrolizumab in cisplatin-ineligible patients with locally advanced and unresectable or metastatic urothelial cancer (KEYNOTE-052): a multicentre, single-arm, phase 2 study. *Lancet Oncol.* **18**, 1483–1492 (2017).
33. Li, X. et al. Demethylase Kdm6a epigenetically promotes IL-6 and IFN-β production in macrophages. *J. Autoimmun.* **80**, 85–94 (2017).
34. Pan, D. et al. A major chromatin regulator determines resistance of tumor cells to T cell-mediated killing. *Science* **359**, 770–775 (2018).
35. Miao, D. et al. Genomic correlates of response to immune checkpoint therapies in clear cell renal cell carcinoma. *Science* **359**, 801–806 (2018).

Acknowledgements

We acknowledge the patients and their families. We particularly thank all the people from the Paramio and Prosper laboratories for discussion and suggestions. We express our acknowledgement to F.X. Real (CNIO) for his critical reading of the manuscript and helpful comments. This study was cofunded by European Regional Development Fund (FEDER) grants from MINECO (no. SAF2015-66015-R to J.M.P. and no. SAF2016-78568-R to J.J.L.), Instituto de Salud Carlos III (RETIC no. RD12/0036/0009 to J.M.P., RTICC no. RD12/0036/0068 to F.P., no. PI14/01867 to F.P., no. PI16/02024 to X.A., no. PI17/00701 to F.P., CIBERONC no. CB16/12/00489 to F.P., CIBERONC no. CB16/12/00228 to J.M.P. and ERANET-TRANSCAN-2 EPICA to F.P.), Departamento de Salud del Gobierno de Navarra no. 40/2016 to X.A. and Gobierno de Navarra Industria (0011-1411-2017-000028; 0011-1411-2017-000029; 0011-1411-2017-000030; Proyecto DIANA to F.P.). We also thank the Fundación Fuentes Dutor (to J.O.) and Fundación La Caixa Hepacare Project (to J.J.L.) for financial support.

Author contributions

C.Segovia, E.S.J.-E., E.M.-M., X.A., F.P. and J.M.P. conceived and designed the study. C.Segovia, E.S.J.-E., E.M.-M., M.M.-F., P.F., J.A.C., M.D. and J.O. developed the methodology. L.G., E.M., A.V.-Z., I.L., C.R., C.Segrelles, L.V.V., O.R., N.C., A.B., C.S.-C., F.F.L.-C., P.F., J.A.C., M.D., F.V., F.G.-R., G.d.V. and D.C. acquired the data and assisted with the experiments. C.Segovia, E.S.J.-E., E.M.-M., P.F., J.A.C., M.D., J.J.L., X.A., F.P. and J.M.P. analyzed and interpreted the data. C.Segovia, E.S.J.-E., E.M.-M., J.J.L., J.O., X.A., F.P. and J.M.P. wrote, reviewed and/or revised the manuscript. L.V.V. and J.M.P. provided administrative, technical and material support (that is, reported or organized the data, built the databases). X.A., F.P. and J.M.P. supervised the study.

Competing interests

The authors declare no competing interests.

Additional information

Extended data is available for this paper at https://doi.org/10.1038/s41591-019-0499-y.

Supplementary information is available for this paper at https://doi.org/10.1038/s41591-019-0499-y.

Reprints and permissions information is available at www.nature.com/reprints.

Correspondence and requests for materials should be addressed to X.A., F.P. or J.M.P.

Peer review information: Javier Carmona was the primary editor on this article and managed its editorial process and peer review in collaboration with the rest of the editorial team.

Publisher's note: Springer Nature remains neutral with regard to jurisdictional claims in published maps and institutional affiliations.

Methods

Clinical data and patient information. Tumor samples and medical records from a cohort of 87 patients with BC treated at Hospital '12 de Octubre' and previously reported[12] (Supplementary Table 5) were analyzed. Samples and clinical information from patients included in this study were provided by the Biobanco i+12 at the Hospital '12 de Octubre', which is integrated in the Spanish Hospital Biobanks Network (RetBioH; www.redbiobancos.es) following standard operation procedures with appropriate approval from the Ethical and Scientific Committee. Metastatic urothelial carcinoma samples were obtained from the primary lesions of 17 patients before they underwent therapy with pembrolizumab. All patients provided written consent before enrolling in the study. All patients received pembrolizumab at doses of 200 mg every 3 weeks until disease progression or until completion of 2 years of therapy regardless of PD-L1 status. Formalin-fixed paraffin-embedded (FFPE) tumor specimens with sufficient viable tumor content were required before the start of the study.

Xenografts in nude mice. All animal experiments were conducted in compliance with the Centro de Investigaciones Energéticas, Medioambientales y Tecnológicas (CIEMAT) guidelines; specific procedures have been approved by the Animal Welfare Department of the Comunidad de Madrid (ProEX 183/15). Eight-week-old female NMRI-FoxN1nu/nu mice (Janvier Labs) were used in the study. RT112 cells were trypsinized and resuspended in a mixture (1:1) of PBS with Matrigel (BD Biosciences); 5×10^6 cells in a 100 µl suspension were implanted subcutaneously in both flanks of each mice ($n=20$). Tumor growth was measured twice a week by digital caliper and tumor volume (mm^3) was calculated using the following formula: $4\pi\times((\text{length}/2)\times(\text{width}/2)^2)/3$. When tumor volume reached between 150 and 250 mm^3, mice were randomized into 4 groups ($n=5$) to receive the different treatments: vehicle (10% DMSO dissolved in PBS; Sigma-Aldrich); CM-272; CDDP; or CM-272 + CDDP. CM-272 was dissolved in PBS and 5 mg kg^{-1} were administrated intraperitoneally 5 d per week. CDDP was injected intraperitoneally once per week at a dose of 6 mg kg^{-1}. After 15 d of treatment, mice were killed when the humane end point was reached, in compliance with the Federation of European Laboratory Animal Science Associations and OEBA-CIEMAT Guidelines. Engrafted tumors were collected and preserved in formalin for further immunohistochemistry staining or in liquid nitrogen for immunoblot analysis.

Transgenic mouse model. All animal experiments were approved by the Animal Ethical Committee and conducted in compliance with the CIEMAT guidelines. Specific procedures were approved by Comunidad Autónoma de Madrid (ProEX 088/15). The *Rb1*$^{loxP/loxP}$, *Trp53*$^{loxP/loxP}$, *Pten*$^{loxP/loxP}$ and *Rbl1*$^{-/-}$ mice were generated by breeding *Rb1*$^{loxP/loxP}$, *Rbl1*$^{-/-}$(ref. [36]) and *Trp53*$^{loxP/loxP}$ and *Pten*$^{loxP/loxP}$ mice[37]. Adenovirus-expressing Cre recombinase under the keratin 5 promoter[38] was obtained from the Viral Vector Production Unit of the Autónoma University of Barcelona and surgically delivered to the bladder lumen as described previously[13,24]. Tumor development was routinely followed by computerized tomography[13] and inspection by palpation. Tissues were collected and processed as reported later in the Methods at the time of the mice being killed. Treatment of these transgenic mice started at the time of tumor detection with CM-272 at doses of 5 mg kg^{-1} intraperitoneally 5 d per week, CDDP once a week at a dose of 3 mg kg^{-1}, anti-PD-L1 once a week for a total of three injections of 200 µg per injection and the different combinations of these agents as described in the main text.

Cell culture and transfection. All cell lines of known genomic characteristics[16] were maintained in culture in DMEM medium supplemented with 1% antibiotic-antimycotic (Gibco) and 10% fetal bovine serum (GE Healthcare) at 37 °C in a humid atmosphere containing 5% CO_2. All cell lines were authenticated by short tandem repeat allele profile and were tested for *Mycoplasma* (MycoAlert Sample Kit; Cambrex). No positive results were obtained. For the knockdown of *EZH2* in RT112 and 5637 cells, cells were transduced with lentivirus-based shRNA TRCN0000353069 and TRCN0000286227 (MISSION shRNA; Sigma-Aldrich). Cells were selected using puromycin resistance (0.5 µg ml^{-1}) for 2 weeks. To overexpress *EZH2*, both lines were transfected using the FuGENE 6 Transfection Reagent (Promega Corporation), with an *EZH2*-coding plasmid reported previously[39]. Transfected cells were selected using hygromycin resistance (250 µg ml^{-1}). Plasmid coding for myristoylated-*p110α*, *E545K* mutant (in pBABE backbone) were generously provided by A. Carnero (IBIS/HUVR/CSIC/Universidad de Sevilla). RT112 transfections were performed as described earlier. Pooled resistant clones were collected for further immunoblot and cell proliferation assays.

Cell proliferation assay. Cell proliferation was analyzed with the CellTiter 96 Aqueous One Solution Cell Proliferation Assay (Promega Corporation) and XTT Cell Proliferation Kit II (Roche). This is a colorimetric method for determining the number of viable cells in proliferation. For the assay, 100 µl of cells were seeded at a density of 5,000 cells per well in 96-well plates in triplicate. Before adding the compounds, adherent cells were allowed to attach to the bottom of the wells for 12 h. In all cases, only the 60 inner wells were used to avoid any border effects. After 24–48 h of treatment with different concentrations, plates with adherent cells were flicked to remove medium. Then, cells were incubated with 100 µl $well^{-1}$ of medium and 20 µl $well^{-1}$ of CellTiter 96 Aqueous One Solution reagent. Cells were incubated for 1–4 h, depending on the cell line, at 37 °C in a humidified, 5% CO_2 atmosphere. Absorbance was recorded at 490 nm using 96-well plate readers until the absorbance of control cells without treatment was around 0.8. Background absorbance was measured in wells with only cell line medium and solution reagent. First, the average of the absorbance from the control wells was subtracted from all other absorbance values. Data were calculated as the percentage of total absorbance of treated cells/absorbance of non-treated cells. The GI_{50} (growth inhibition of 50% of cells) values of the different compounds were determined using non-linear regression plots with Prism 6 (GraphPad Software).

Cell cycle analysis. For cell cycle analysis, 250,000 cells were treated for 24 and 48 h with a GI_{50} concentration of CM-272 (700 nM for RT112 and 880 nM for 5637 cells). Then, cells were washed twice with PBS and resuspended in 0.2% Tween 20 in PBS and 0.5 mg ml^{-1} RnaseA (ribonuclease A type III-A from bovine pancreas; catalog no. R5125; Sigma-Aldrich) and incubated for 30 min at 37 °C. Subsequently, cells were stained with 25 µg ml^{-1} of propidium iodide (catalog no. P4170; Sigma-Aldrich) and analyzed using a BD FACSCalibur flow cytometer (BD Biosciences).

Apoptosis assay. For the apoptosis assay, 100,000 cells were treated for 24 h with CM-272 at different concentrations (GI_{25}, GI_{50} and GI_{75}). The FITC Annexin V Apoptosis Detection Kit I (catalog no. 556547; BD Biosciences) was used according to the manufacturer's instructions, with some modifications. First, cells were washed twice with PBS and resuspended in 1X Binding Buffer at a concentration of 1×10^6 cells ml^{-1}. Then, 1 µl of FITC Annexin V (AV) antibody and 2 µl of propidium iodide were added and incubated for 15 min at room temperature in the dark. Finally, 400 µl of 1X Binding Buffer were added to each tube and analyzed by flow cytometry within 1 h. We represented the addition of FITC AV^+ and propidium $iodide^-$ cells (early apoptosis) and FITC AV^+ and propidium $iodide^+$ cells (end stage apoptosis, death).

Combination assays. To calculate the combination index values, RT112 and 5637 growth inhibition was determined at multiple concentrations of G9a inhibitor (A-366) (12.5, 25, 50 and 100 µM) in combination with varied concentrations of decitabine (12.5, 25, 50 and 100 µM) or EZH2 inhibitor (GSK-126) or various concentrations of CM-272 and CDDP (Selleck Chemicals). Briefly, 5,000 cells were cultured in duplicate in a 96-well plate. Cells were added at 80 µl per well and the different concentrations of the compounds were added at 10 µl, the final volume being 100 µl. We prepared serial dilutions 10 times concentrated and 10 µl of each dilution was added to each well. After adding the compounds, cells were incubated for 48 h and then processed for MTS assays using the CellTiter 96 Aqueous One Solution Cell Proliferation Assay (catalog no. G3580: Promega Corporation) according to the manufacturer's instructions. The resulting data were analyzed according to the method described by Chou and Talalay[40] (CalcuSyn software V2; Biosoft). The combination index was used to determine whether the effect of drug combinations were synergistic, additive or antagonistic. Synergy, additivity and antagonism were defined by a combination index <1, 1 and >1, respectively.

For interference studies using siRNAs against *G9a* and *DNMT1*, RT112 and 5637 cells (1.25×10^5 and 1×10^5, respectively) were seeded onto 6-well plates in RPMI 1640 medium lacking antibiotics. Once cultured, cells achieved a confluency of 30–50%; cells were transfected with 50 nM of *G9a* or *DNMT1* siRNA or Silencer Select Negative Control-1 (Ambion) using lipofectamine 2000 (Invitrogen) and opti-MEM medium (Gibco), according to the manufacturer's instruction. Cells were incubated at 37 °C in a humidified atmosphere and 5% CO_2 for further 48 h and then cell proliferation was analyzed (siG9a: CGCUGAUUUUCGAGUGUAA; siDNMT1: DNMT1 siRNA; catalog no. sc35204; Santa Cruz Biotechnology).

Western blot. Cell and tumor samples were disrupted by freeze–thawing cycles in lysis buffer (20 mM HEPES, pH 7.5, 1% Triton X-100, 40 mM β-glycerophosphate, 100 mM NaCl, 20 mM $MgCl_2$, 10 mM EGTA) supplemented with protease and phosphatase inhibitor cocktails (Complete Mini, catalog no. 11836153301; Roche) and centrifuged to obtain supernatant containing total protein; 30 µg of protein per sample were resolved in 4–12% NuPAGE gels (Invitrogen) and transferred to nitrocellulose membranes. Membranes were blocked with 5% non-fat dry milk in 0.1% Tween 20 PBS and incubated with the appropriate antibodies used against: G9a (catalog no. ab180815; Abcam); EZH2 (catalog no. MAB9542; Abnova); H3K9me2 (catalog no. ab1220; Abcam); H3K27me3 (catalog no. 07-449; Merck Millipore); H3K9me3 (catalog no. ab8898; Abcam); phospho-Akt (Ser473) (catalog no. 4060; Cell Signaling Technology); cleaved caspase-3 (Asp175; catalog no. 9661S; Cell Signaling Technology); cleaved anti-PARP (catalog no. 611039; BD Biosciences); anti-LC3B antibodies (catalog no. ab48394; Abcam) that predict the forms LCI/LCII; Rb total (catalog no. 554136; BD Biosciences); p53 (catalog no. NCL-L-p53-CM5p; Novocastra); PTEN (catalog no. SC 6818; Santa Cruz Biotechnology); ERK1 total (catalog no. SC-94; Santa Cruz Biotechnology); phospho-ERK1/2 (Thr202/Tyr204) (catalog no. 4370; Cell Signaling Technology); Akt1/2 (catalog no. SC 1619; Santa Cruz Biotechnology); Stat3 (catalog no. 4904; Cell Signaling Technology); phospho-Stat3 (Tyr705) (catalog no. 9131; Cell Signaling Technology); ribosomal S6 (catalog no. 2317; Cell Signaling Technology); and phospho-S6 (Ser 235/236) (catalog no. 2211; Cell Signaling Technology).

Loading was controlled by using anti-GAPDH (catalog no. sc-25778; Santa Cruz Biotechnology) or anti-actin (catalog no. sc-1616; Santa Cruz Biotechnology) antibodies. The full uncropped blots are shown in the Source data associated with this paper.

Histone extractions. After 24, 48, 72 and 96 h of treatment, cells were washed twice with PBS, and centrifuged for the last time at 4,000 r.p.m. for 10 min at 4 °C. Histone extraction was performed as recommended by Upstate Biotechnology. Briefly, cells were homogenized in 5 volumes of lysis buffer and HCl was added to a final concentration of 0.2 M. After incubation on ice for 30 min, the homogenate was centrifuged at 11,000*g* for 10 min at 4 °C; the supernatant was first dialyzed twice against 0.1 M glacial acetic acid (1 h each time) and then three times against water for 1 h, 3 h and overnight, respectively. The histone concentration in the extract was measured using the Bradford dye-binding assay; 10 µg of histone was separated on a 15% SDS–polyacrylamide gel electrophoresis gel and transferred to a nitrocellulose membrane. The membrane, after being blocked with Tropix I-block blocking reagent (catalog no. AI300; Tropix) in PBS with 0.1% Tween 20 and 0.02 NaN_3, was incubated with primary mouse monoclonal antibody against H3K9me2 (catalog no. ab1220; Abcam) diluted 1:2,000 overnight at 4 °C and then with alkaline phosphatase-conjugated secondary antibodies. Bound antibodies were revealed by a chemiluminescent reagent (Tropix) and detected using Hyperfilm-enhanced chemiluminescence. Total H3 was used as a loading control (diluted 1:50,000 overnight at 4 °C or for 1 h at room temperature; anti-histone H3, CT, pan, rabbit polyclonal, catalog no. 07-690; Merck Millipore).

Dot blot. After 24, 48, 72 and 96 h of treatment, cells were washed twice with PBS and genomic DNA was extracted with a DNA kit (NucleoSpin Tissue, catalog no. 74095250; Macherey-Nagel) according to the manufacturer's instructions. DNA purity and concentration was measured using a NanoDrop spectrophotometer (Thermo Fisher Scientific); 500 ng of genomic DNA was loaded onto a nitrocellulose membrane (Amersham Hybond-N+, catalog no. RPN203B; GE Healthcare Life Sciences), pre-wetted in 6X SSC for 10 min, using the Bio-Dot microfiltration apparatus (catalog no. 170-6545; Bio-Rad) according to the manufacturer's instructions. Then, the membrane was incubated with 2X SSC for 5 min and was cross-linked for 2 h at 80 °C. After being blocked with Tropix I-block blocking reagent in PBS with 0.1% Tween 20 and 0.02 NaN_3, the membrane was incubated with the primary antibody against 5-methylcytosine (monoclonal antibody 5-methylcytidine, catalog no. BI-MECY-1000; Kaneka Eurogentec) diluted 1:4,000 overnight at 4 °C and then with alkaline phosphatase-conjugated secondary antibody. Bound antibodies were revealed by a chemiluminescent reagent (Tropix) and detected using Hyperfilm-enhanced chemiluminescence.

Quantitative PCR with reverse transcription (RT–qPCR). Expression of *IFI44L*, *EPSTI1*, *OASL*, *IFI6*, *USP18, ABTB, MER21C, MLTA10, MTL2B4, ERVL, PD-L1, PD-1* and *CTLA4* was analyzed by RT–qPCR in RT112 and 5637 cell lines after 48 h of CM-272 treatment. First, cDNA was synthesized from 1 µg total RNA using the PrimeScript RT Reagent Kit (Perfect Real Time) (catalog no. RR037A; according to TaKaRa) according to the manufacturer's instructions. The quality of cDNA was checked with a multiplex PCR that amplifies the *PBGD*, *ABL*, *BCR* and *B2M* genes. RT–qPCR was performed in a 7300 Real-Time PCR System (Applied Biosystems), using 20 ng of cDNA in 2 µl and 1 µl of each primer at the concentration specified in Supplementary Table 6, and 6 µl of SYBR Green PCR Master Mix (catalog no. 4334973; Applied Biosystems) in 12 µl reaction volume. The following program conditions were applied for RT–qPCR: 50 °C for 2 min, 95 °C for 60 s followed by 45 cycles at 95 °C for 15 s and 60 °C for 60 s; melting program, one cycle at 95 °C for 15 s, 40 °C for 60 s and 95 °C for 15 s. The relative expression of each gene was quantified by the $\log_2^{(\Delta\Delta Ct)}$ method using the *GUS* gene as an endogenous control.

Total RNA from human tumor samples was isolated with the miRNeasy Mini Kit (QIAGEN) according to the manufacturer's instructions and DNA was eliminated (Rnase-Free Dnase Set; QIAGEN). Reverse transcription was performed with the Omniscript RT Kit (QIAGEN) using 50 ng of total RNA and specific primers for G9a. *TBP* was used as the reference gene for normalization. PCR was performed in a 7500 Fast Real-Time PCR System (Applied Biosystems) using GoTaq PCR Master Mix (Promega Corporation) and 1 µl of cDNA as a template. Melting curves were performed to verify specificity and the absence of primer dimers. Reaction efficiency was calculated for each primer combination.

Quantitative chromatin immunoprecipitation (ChIP). For ChIP analysis, RT112 and 5637 cells were treated with CM-272 (700 nM for RT112 and 880 nM for 5637) for 48 h. The ChIP assay was performed as described previously[41]. Quantitative ChIP was performed in a 7300 Real-Time PCR System using 0.5 µl of each 2 µM primer shown in Supplementary Table 7 (final concentration of 0.083 µM), 6 µl of SYBR Green PCR Master Mix in 12 µl reaction volume. In the case of *PD-L1*, 1 µl of each 10 µM primer was used (final concentration of 0.83 µM). The amount of DNA varies among genes and is specified in Supplementary Table 7. The following program conditions were applied for quantitative ChIP: 50 °C for 2 min, 95 °C for 60 s followed by 45 cycles at 95 °C for 15 s and 60 °C for 60 s; melting program, one cycle at 95 °C for 15 s, 40 °C for 60 s and 95 °C for 15 s. The H3K9me2 percentage of each gene was quantified as follows: $((2^{(\Delta\Delta Ct)}$ CM-272 sample/$2^{(\Delta\Delta Ct)}$ control)*100).

Immunofluorescence of dsRNA. Fifty thousand cells from each of the RT112 and 5637 cell lines were plated on a glass coverslip in a 12-well plate for 24 h and subsequently treated with CM-272 (700 nM for RT112 and 880 nM for 5637) for 48 h. After washing the cells with PBS, cells were fixed in 4% paraformaldehyde in PBS (Thermo Fisher Scientific) for 15 min, permeabilized with PBS containing 0.5% Triton X-100 for 15 min and blocked with 0.25% BSA in PBS for 1 h at room temperature. Thereafter, cells were incubated with the mouse monoclonal antibody J2 (catalog no. 10010200; SCICONS) to detect dsRNA (1:150 dilution in PBS containing 0.25% BSA) for 1 h. Cells were washed three times for 5 min each time in tris-buffered saline with Tween 20 (TBST) before incubation with secondary antibody anti-mouse IgG Cy3 conjugate (catalog no. C2181, Sigma-Aldrich; diluted 1:250 in PBS containing 0.25% BSA) for 1 h. Then, cells were washed three times, for 5 min each time, in TBST. The coverslips were inverted onto VECTASHIELD antifade mounting medium with DAPI (Vector Laboratories) on microscope slides, viewed with a Zeiss digital confocal microscope and photographed.

Determination of cell surface-exposed calreticulin by FACS. RT112 cells were incubated for 48 h with or without CM-272 (250 nM). Then, cells were collected and washed with ice-cold PBS, then incubated with a calreticulin-specific antibody (catalog no. ab2907, Abcam) diluted in cold blocking buffer (5% BSA in PBS) for 30 min on ice, washed and incubated with an FITC-conjugated antibody (catalog no. 1262, Sigma-Aldrich) in blocking buffer for 30 min. Thereafter, cells were washed, stained with 1 µg ml^{-1} TO-PRO-3 Iodide (Thermo Fisher Scientific) in cold PBS for 5 min, and analyzed by means of a FACScalibur cytofluorometer (BD Biosciences). First-line statistical analyses were performed with the CellQuest software (BD Biosciences), when gating on TO-PRO-3 Iodide-negative events characterized by normal forward and side scatter (living cells).

Determination of extracellular HMGB1 concentrations. Cells were incubated for 48 h with or without CM-272 (250 nM). The extracellular HMGB1 from 48 h cell culture supernatants was quantified using the HMGB1 ELISA Kit II (Shino-Test Corporation) according to the manufacturer's instructions.

Tissue microarray and immunohistochemistry. For immunohistochemical analyses, human and mouse tissues were fixed in buffered formalin and embedded in paraffin. Slides were deparaffinized and antigen retrieval was performed with citric acid buffer (pH 6) using a pressure cooker (Dako). Endogenous peroxidase was inhibited with hydrogen peroxide (0.3%) in methanol. Sections were blocked with 5% normal horse serum for 30 min and then washed with sterile PBS (pH 7.5) before incubation with the following appropriate primary antibodies diluted in PBS/BSA against G9a, EZH2, H3K27me3, H3K9me2, cleaved caspase-3, LC3B, CD163 (catalog no. ab74604; Abcam), CD8 (catalog no. ab203035; Abcam) and FITC mouse anti-mouse NK-1.1 antibodies (catalog no. 553164; BD Biosciences). The human bladder samples and the construction of tissue microarrays have been described elsewhere[12]. The tissue microarrays were stained with H&E and were reviewed to confirm the presence of representative tumor tissue (at least 70% of tumor cells). Double-blind scoring of the results and selection of the thresholds, internal controls for reactivity of each antibody and tissue controls for the series were done according to previously published methods[1]. To monitor cell proliferation in tissues, mice were injected intraperitoneally with BrdU (0.1 mg g^{-1} weight in 0.9% NaCl; Roche) 1 h before they were killed. BrdU incorporation was monitored in formalin-fixed sections using an anti-BrdU antibody (Roche).

Whole transcriptome analyses. Total RNA was extracted from control and CM-272-treated (GI_{50}) cells using triplicates as stated earlier. cDNA from 12 ng total RNA was generated, fragmented, biotinylated and hybridized to the GeneChip Human Transcriptome Array 2.0 arrays (Affymetrix). Total RNA from control and macrodissected tumors from transgenic mice was extracted with the miRNeasy FFPE Kit (QIAGEN). cDNA from 12 ng total RNA was generated, fragmented, biotinylated and hybridized to the GeneChip Mouse Transcriptome Array 1.0 (Affymetrix). cDNA was generated, fragmented, biotinylated and hybridized to the corresponding array. Human Transcriptome Array 2.0 or Clariom D Mouse Arrays (Affymetrix) were washed and stained on a GeneChip Fluidics Station 450 (Affymetrix); scanning was carried out with the GeneChip Scanner 3000 7 G and image analysis was performed with the GeneChip Command Console Scan Control (Affymetrix). Expression data were normalized; background and batch were corrected using Guanine Cytosine Count Normalization and Signal Space Transformation before being summarized using the Robust Multi-Array Average algorithm and batch correction using the ComBat method implemented in the Affymetrix Expression Console Software. Datasets have been deposited in the Gene Expression Omibus with accession numbers GSE115544, GSE115485 and GSE111636. Hierarchical clustering was performed using Euclidean distance as the similarity metric, with average linkage clustering following the Pearson correlation using Multiple Experiment Viewer software[42]. Clustering results were visualized by the heatmaps generated. GSEA was performed using the MSignature and Motif databases[43]. Identification of transcription factor binding was performed using the ChIP enrichment analysis of the Enrichr webtool (http://amp.pharm.mssm.edu/Enrichr/)[44].

Analysis of NKG2D ligands in RT112 and 5637 cell lines by flow cytometry. Cell lines with 80–90% confluence were treated with the inhibitor *G9a*/*EZH2* for 24 h; adherent cells were detached with trypsin and washed in PBS/BSA. Then, 1×10^5 cells were labeled with the follow monoclonal antibodies for NKG2D ligands (all Novus Biologicals): MICA (catalog no. 159227); MICB (catalog no. 236511); ULBP1 (catalog no. 170818); ULBP-3 (catalog no. 166510); ULBP-4 (catalog no. 709116) and ULBP-2/5/6-PE (catalog no. 165903). After 30 min at 4 °C, cells were washed and resuspended in PBS/PBA with DAPI to discard dead cells in the flow cytometry analysis. The fold change of mean fluorescence intensity (MFI) for each NKG2D ligand was evaluated according to its corresponding level in the untreated culture performed in parallel.

Analysis of PD-L1, PD-1 and cytotoxic T-lymphocyte protein 4 (CTLA4) in the RT112 cell line by flow cytometry. After 48 h of treatment with 700 nM CM-272, 2×10^5 RT112 cells were labeled for 15 min at room temperature in the dark with the following monoclonal antibodies or appropriate conjugated isotype controls: APC-PD-L1 mouse IgG2b (catalog no. 329708; BioLegend); Brilliant Violet 421-PD1 mouse IgG1 (catalog no. 329919, BioLegend); PE-CTLA4 mouse IgG2a (catalog no. 555853; BD Biosciences); FITC annexin V (catalog no. ANXVF-200T; IMMUNOSTEP); APC mouse IgG1 isotype control (catalog no. 400119; BioLegend); Brilliant Violet 421 mouse IgG1 isotype control (catalog no. 400158; BioLegend) or PE mouse IgG2a isotype control (catalog no. 400211; BioLegend). Then, cells were washed with PBS and resuspended in annexin V binding buffer. Acquired data were analyzed using FlowJo v.10 (FlowJo LLC). Annexin V^+ cells were discarded in the analysis. Data are presented as the fold change of MFI for each protein compared with the isotype controls and untreated cells.

Selectivity of CM-272 against *EZH2* mutations. Selectivity of CM-272 against *EZH2* mutations (A677G, A738T, Y641S, P132S, Y641C, Y641F, Y641H and Y641N) and EZH2–embryonic ectoderm development (EED) interaction was performed by BPS Bioscience (http://www.bpsbioscience.com/index.ph). Binding experiments were performed in duplicate at a test concentration of 10 µM.

DNA methylation analysis. The DNA methylation status of the *PD-L1* promoter was analyzed by pyrosequencing technique. First, the RT112 cell line was treated for 48 h with 700 nM of CM-272. Cells were washed twice with PBS and genomic DNA was extracted using a DNA kit (Nucleo Spin Tissue) according to the manufacturer's instructions. DNA purity and concentration were measured using a NanoDrop spectrophotometer and 1 µg of genomic DNA was treated and modified using the CpGenome DNA Modification Kit (catalog no. S7820; Sigma-Aldrich) according to the manufacturer's instructions.

After bisulfite modification, 'hot start' PCR (PyroMark PCR Kit, catalog no. 978703; QIAGEN) was performed with denaturalization at 95 °C for 15 min, followed by 45 cycles consisting of denaturation at 94 °C for 1 min, annealing at 55 °C for 1 min and extension at 72 °C for 1 min followed by a final 10 min extension. This PCR was performed using 2 µl of modified DNA, 12.5 µl of 2X Buffer and 1 µl of 10 µM of each specific primer (final concentration of 0.4 µM) (PD-L1 forward: 5′-AAAAAGAAAAGGGAGTATATAGGTA-3′ and PD-L1 reverse: 5′-biotin-AATAAATAAACCCAAAATAACAAAC-3′) in a final volume of 25 µl. The resulting biotinylated PCR products were immobilized to streptavidin Sepharose High Performance Beads (GE Healthcare) and processed to yield high-quality single-stranded DNA using the PyroMark Vacuum Prep Workstation (QIAGEN), according to the manufacturer's instructions. The pyrosequencing reactions were performed using the Pyromark ID 1.0.9 (QIAGEN) and sequence analysis was performed using the PyroQ-CpG analysis software (QIAGEN).

Statistical analysis. Comparisons were made with the Mann–Whitney *U*-test (for unpaired samples without a normal distribution) and the Student's *t*-test (for paired samples showing Gaussian distribution). Survival analyses (recurrence-free) according to various variables were performed using the Kaplan–Meier method and differences between the different groups of patients or mice were tested with the log-rank test. The correlation between *G9a* and *EZH2* mRNA expression was calculated with Pearson correlation. Contingency analyses were performed with Fisher's exact test (*F*-test). Discrimination between samples showing increased or decreased tumor/normal relative expression of either gene or microRNA expression was made using the median. SPSS v.17.0 (IBM Corporation) and Prism 6.0 were used. $P < 0.05$ was considered significant.

Reporting Summary. Further information on research design is available in the Nature Research Reporting Summary linked to this article.

Data availability

Datasets have been deposited in the Gene Expression Omnibus with accession nos. GSE115544, GSE115485 and GSE111636. Full uncropped blots are available as Source data.

References

36. Costa, C. et al. A novel tumor suppressor network in squamous malignancies. *Sci. Rep.* **2**, 828 (2012).
37. Moral, M. et al. Akt activation synergizes with *Trp53* loss in oral epithelium to produce a novel mouse model for head and neck squamous cell carcinoma. *Cancer Res.* **69**, 1099–1108 (2009).
38. Ramírez, A., Bravo, A., Jorcano, J. L. & Vidal, M. Sequences 5′ of the bovine keratin 5 gene direct tissue- and cell-type-specific expression of a *lacZ* gene in the adult and during development. *Differentiation* **58**, 53–64 (1994).
39. Martínez-Fernández, M. et al. A Polycomb-mir200 loop regulates clinical outcome in bladder cancer. *Oncotarget* **6**, 42258–42275 (2015).
40. Chou, T. C. & Talalay, P. Quantitative analysis of dose–effect relationships: the combined effects of multiple drugs or enzyme inhibitors. *Adv. Enzym. Regul.* **22**, 27–55 (1984).
41. Roman-Gomez, J. et al. Epigenetic regulation of microRNAs in acute lymphoblastic leukemia. *J. Clin. Oncol.* **27**, 1316–1322 (2009).
42. Saeed, A. I. et al. TM4: a free, open-source system for microarray data management and analysis. *Biotechniques* **34**, 374–378 (2003).
43. Subramanian, A. et al. Gene set enrichment analysis: a knowledge-based approach for interpreting genome-wide expression profiles. *Proc. Natl Acad. Sci. USA* **102**, 15545–15550 (2005).
44. Chen, E. Y. et al. Enrichr: interactive and collaborative HTML5 gene list enrichment analysis tool. *BMC Bioinformatics* **14**, 128 (2013).

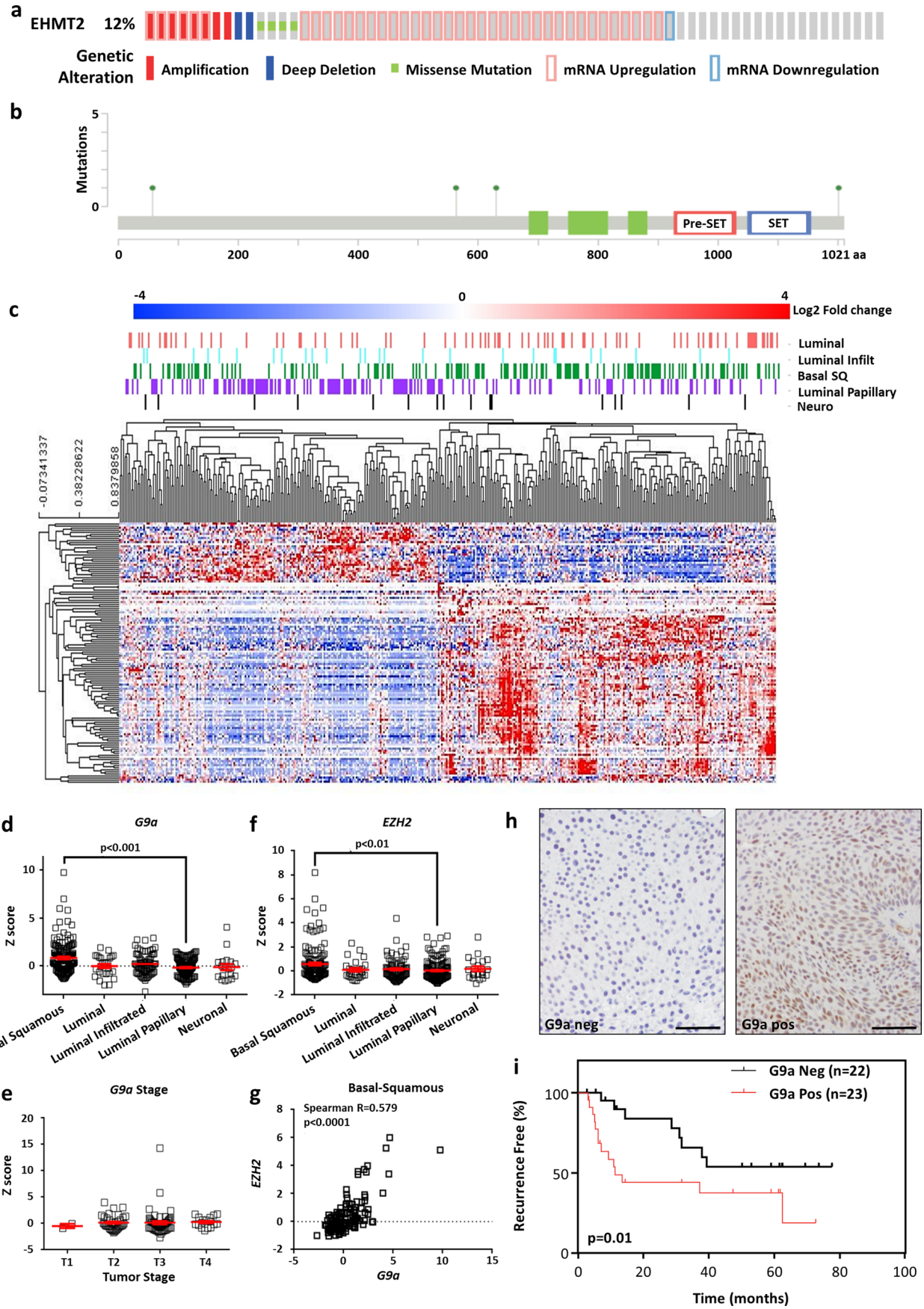

Extended Data Fig. 1 | see figure caption on next page.

Extended Data Fig. 1 | Alterations in *G9a* gene in the TCGA BC database. a, Summary of *G9a* gene alterations observed in the TCGA database. Classification was made according to *z*-scores of mRNA expression (RNA-Seq V2 RSEM) with a threshold ± 2.0. **b**, Summary of *G9a* gene mutations localization reported in the TCGA database. **c**, Heatmap showing the supervised classification of genes bound by *G9a* according to the different TCGA BC molecular subtypes. **d**, Summary of *G9a* gene expression in the different TCGA molecular subtypes according to *z*-scores of mRNA expression (RNA-Seq V2 RSEM). **e**, Summary of *G9a* gene expression at different tumor stages from the TCGA database. **f**, Summary of *EZH2* gene expression in the different TCGA molecular subtypes according to *z*-scores of mRNA expression (RNA-Seq V2 RSEM). **g**, Correlation analyses between *G9a* and *EZH2* gene expression from TCGA database. $n = 404$ patients. **h**, Representative immunohistochemistry images of *G9a* expression in NMIBC samples showing a negative (left panel) and positive (right panel) example. Histological analyses and staining were performed in all clinical samples (patient), scoring at least two different sections from each tumor. Bar, 150 µm. **i**, Kaplan–Meier graph showing recurrence according to G9a protein staining in human NMIBC samples. The *P* value was determined by the log-rank test. **d**–**f**, $n = 404$ patients. Data are represented as the mean ± s.e.m. The *P* value was estimated using a two-sided *t*-test.

a

Cell Line	Gene									CM272 (IC50)
	TP53	RB1	EZH2	EHMT2	KDM5A	ARID1A	KDM6A	PIK3CA	FGFR3	
MGH U3	P72R	WT	WT	WT	WT	WT	WT	WT	Y373C	0.28μM
RT112	R248Q/S183*	WT	WT	WT	WT	WT	P1191fs	WT	WT	0.70μM
UMU UC1	p1525	WT	WT	WT	WT	WT	Q1281*	WT	WT	0.70μM
RT4	WT	WT	WT	WT	WT	3´UTR	WT	WT	WT	0.85μM
5637	R280T	Y325*	WT	WT	W139*	WT	WT	WT	WT	0.88μM
J82	E271K	1703_splice	WT	WT	WT	WT	C1413Y	P124L	K652E	>10μM
253J	WT	WT	WT	WT	WT	WT	WT	E545G	WT	>10μM

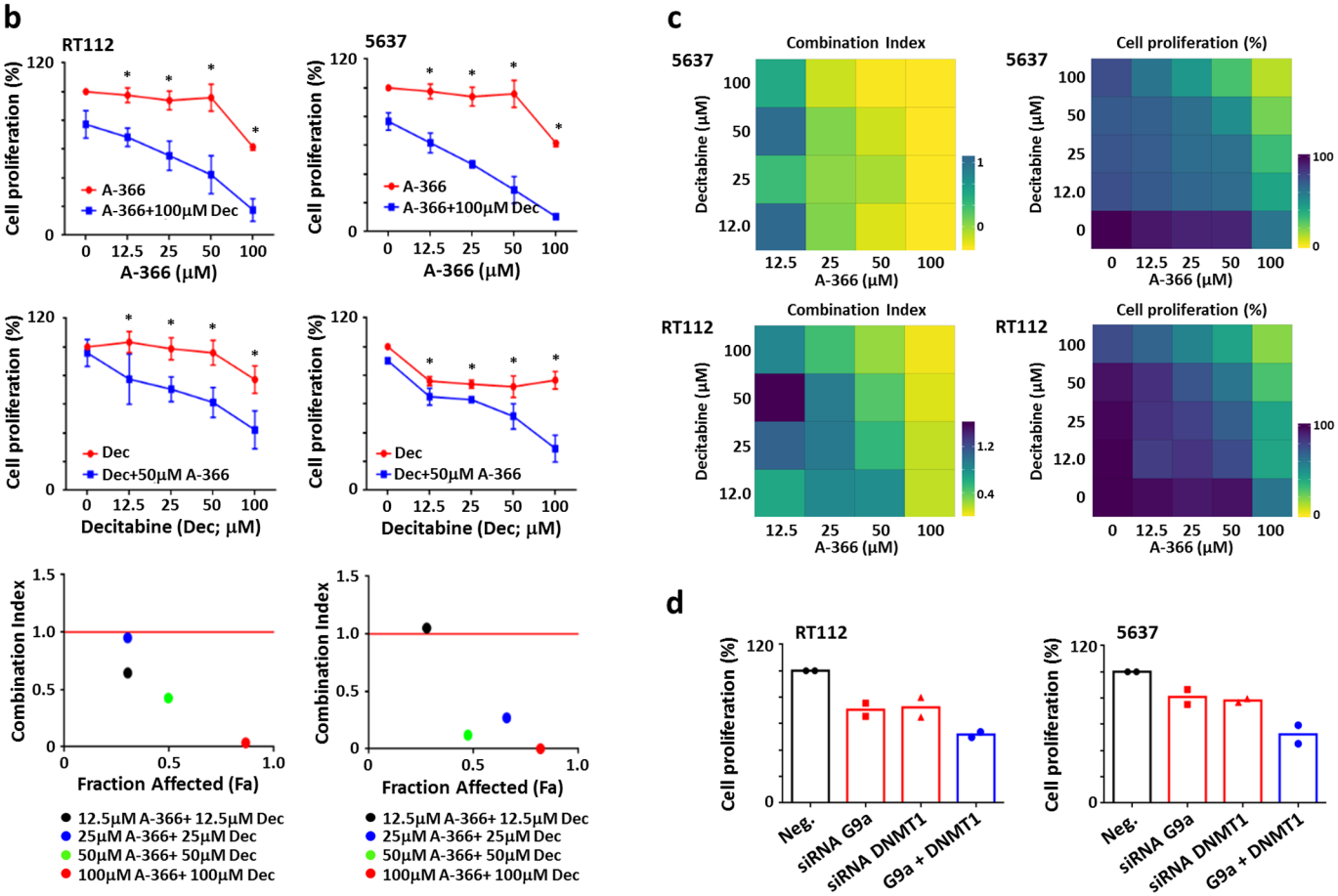

Extended Data Fig. 2 | Effect of inhibition of *G9a* and *DNMT1* in BC cells. a, Summary of gene mutations and GI_{50} values for CM-272 in BC cell lines. **b**, Proliferation of RT112 and 5637 cell lines after treatment with A-366 or decitabine alone or in combination at different doses. A combination index lower than 1 indicates a synergistic effect as defined by Chou and Talalay[36] (combination index > 0.85, slight or no synergism; combination index between 0.7 and 0.85, moderate synergism; combination index between 0.3 and 0.7, synergism; combination index between 0.1 and 0.3, strong synergism). Combination doses were based on GI_{50} values for A-366 and decitabine against the tested cell line (the GI_{50} is >50 μM in both cases). *$P < 0.05$. One-tailed Mann–Whitney *U*-test. $n = 3$ independent experiments. Data are represented as the mean ± s.d. **c**, Heatmaps of cell proliferation of the 5637 and RT112 cell lines after treatment with A-366 or decitabine alone or in combination at different doses (right). Heatmaps of combination indexes (left). **d**, Proliferation of RT112 and 5637 cells after treatment with specific siRNAs against *G9a* and *DNMT1* alone or in combination. Data are represented as the mean ± s.d. $n = 2$ independent experiments.

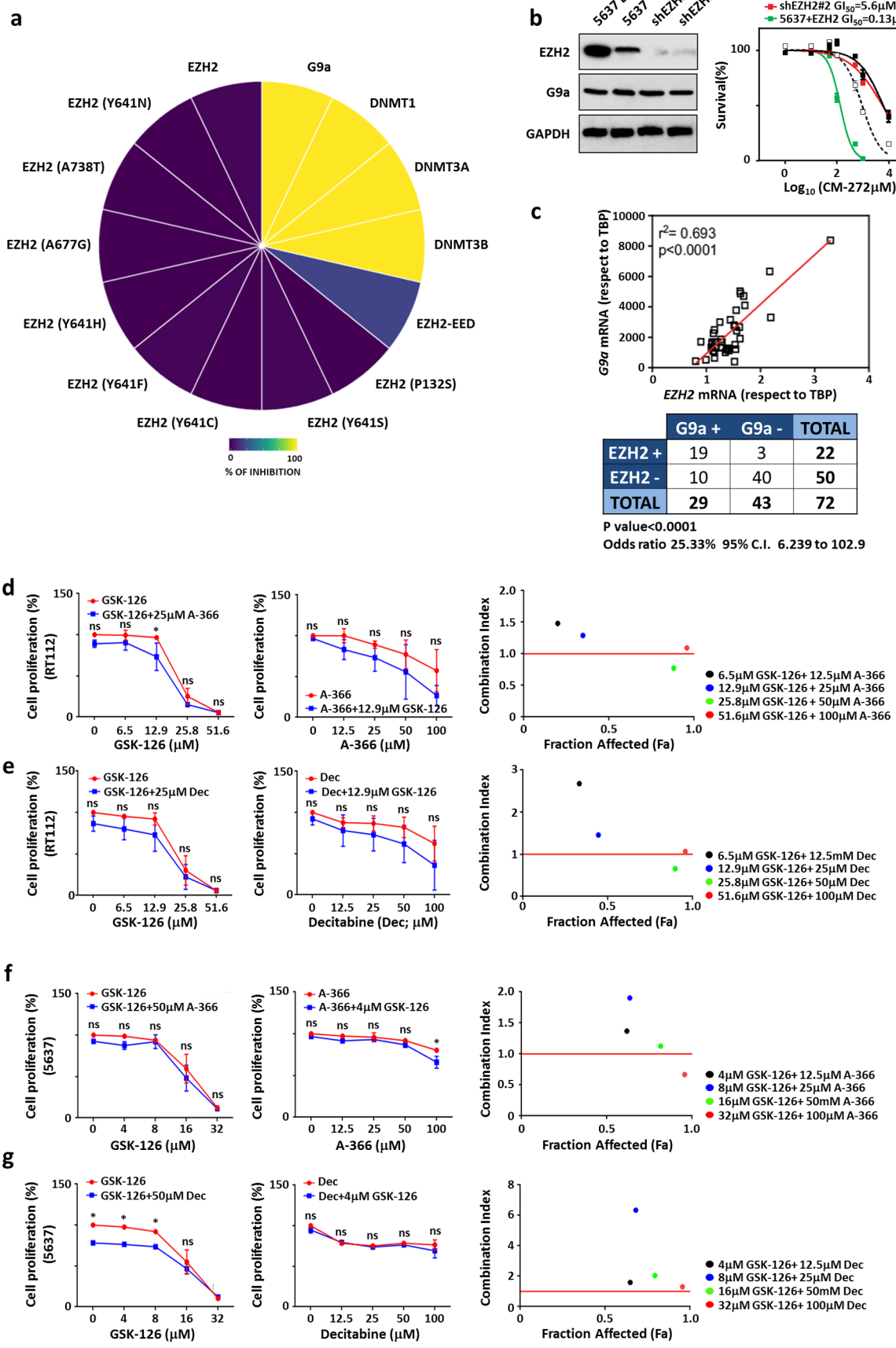

Extended Data Fig. 3 | see figure caption on next page.

Extended Data Fig. 3 | Effect of *EZH2* inhibition in BC cells. a, Effect of CM-272 on the enzymatic activities of distinct human *EZH2* mutants, EZH2–EED binding activity, *G9a* and *DNMT* using in vitro assays. In this study, we included the recombinant human EZH2 A677G, A738T, Y641S, P132S, Y641C, Y641F, Y641H and Y641N. **b**, Immunoblot showing the expression of the cited proteins or histone marks in parental 5637 cells or derivatives overexpressing 5637 EZH2 or on EZH2 knockdown (two different shRNAs denoting shEzh2#1 and shEzh2#2 were used) (left panel). A representative example of two independent experiments is shown. Full uncropped blots are available as Source data. Proliferation of parental RT112 cells or derivatives (overexpression or knockdown of EZH2) after treatment with CM-272 (right panel). Results are the mean ± s.e.m. of three independent experiments. **c**, Correlation between *G9a* and *EZH2* RNA (upper panel) and protein expression (lower panel) in BC patients. Correlation was calculated using Spearman correlation analysis. $n = 55$ patients. **d**–**g**, Proliferation of RT112 (**d**,**e**) or 5637 cells (**f**,**g**) after treatment with GSK-126 (EZH2 inhibitor) alone or in combination with A-366 (**d**,**f**) or decitabine (**e**,**g**). At several tested concentrations, the combination index is >1 according to the range of combinations indexes defined by Chou and Talalay[40]. The combination study set-up was based on GI_{50} values for the assayed molecules. The asterisks show the *P* values of one-tailed Mann–Whitney *U*-tests ($^*P < 0.05$). The results represent the mean ± s.d. of three independent experiments.

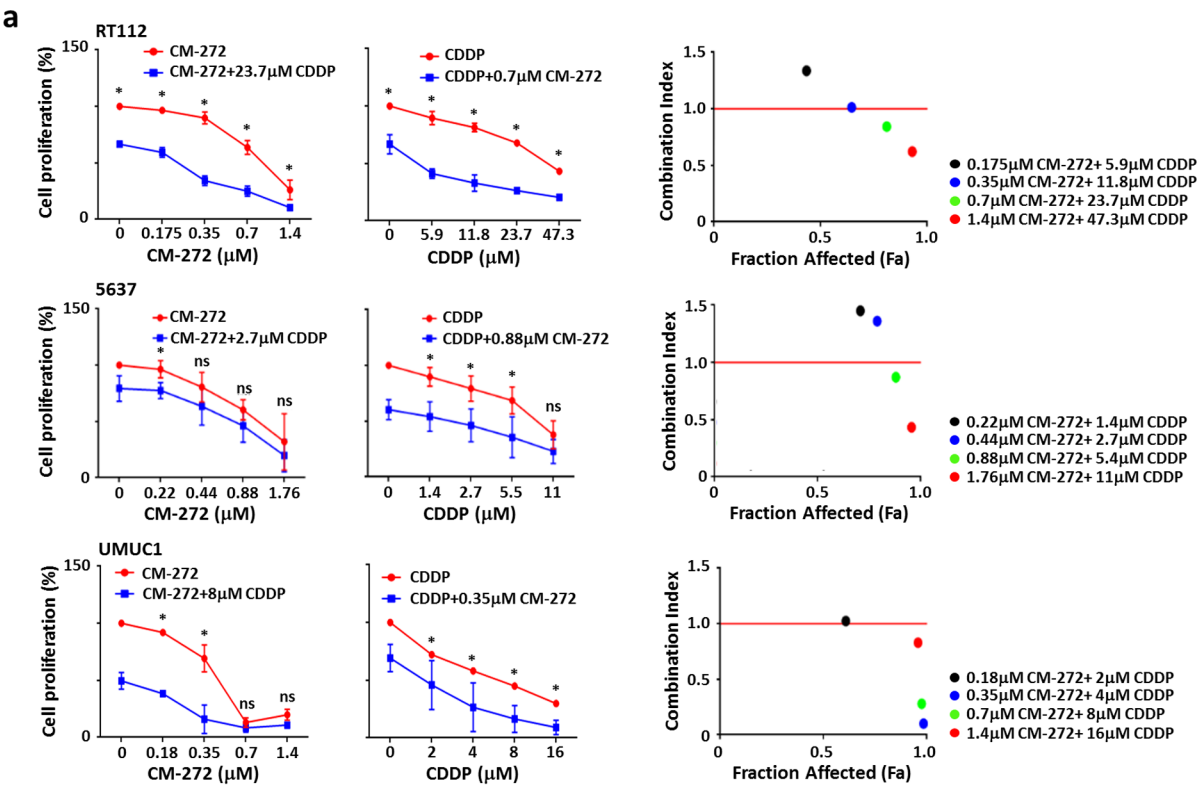

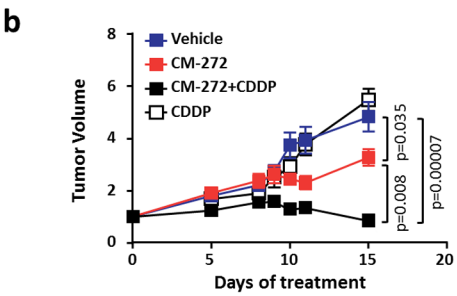

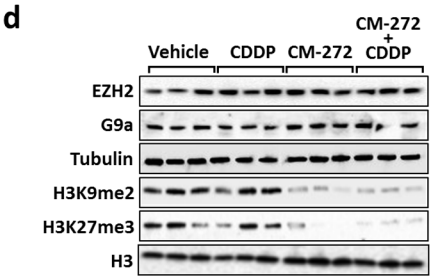

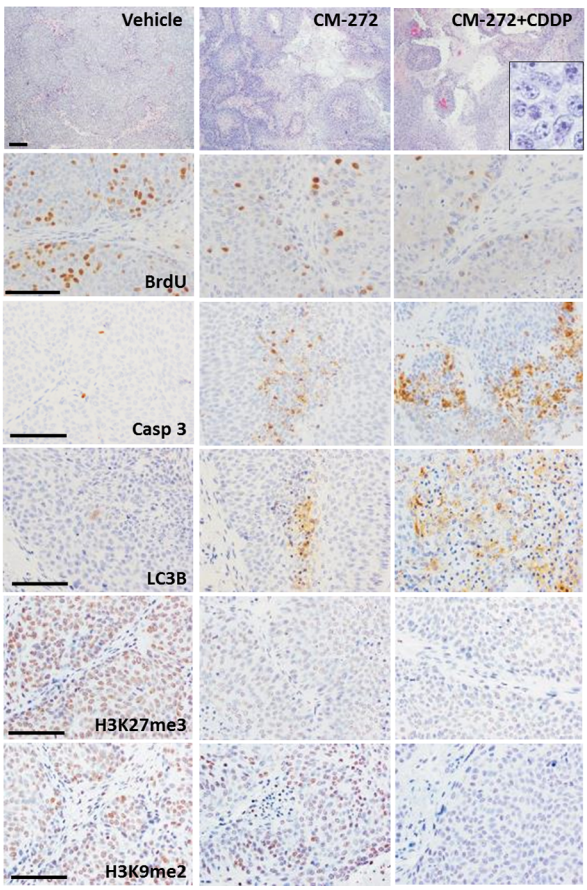

Extended Data Fig. 4 | see figure caption on next page.

Extended Data Fig. 4 | In vitro and in vivo activity of CM-272 and CDDP in BC cells. a, Cell proliferation of BC cells (RT112, 5637 and UMUC1) after treatment with CM-272 alone or in combination with CDDP, showing a synergistic effect (combination index <1 as defined by Chou and Talalay[36]). The asterisks show the *P* values of a one-tailed Mann–Whitney *U*-test (*$P < 0.05$). $n = 3$ independent experiments. The error bars indicate the s.d. **b**, RT112 cells (5×10^6) were subcutaneously implanted in the flanks of nude mice (5 per group). When tumors reached 150–250 mm^3, mice were treated intraperitoneally with CM-272 (5 mg kg^{-1} 5 d per week), CDDP (6 mg kg^{-1} once a week) or both compounds for 2 weeks. Tumor volume was related to baseline volume before treatment. Data are represented as the mean ± s.e.m. *P* values were determined by a one-sided Mann–Whitney *U*-test. **c**, H&E-stained and immunohistochemistry images showing the expression of the cited proteins or histone marks in tumor xenografts corresponding to the cited treatment groups. The representative images of at least 6 independent samples obtained from 3–6 different animals are shown. Scale bars, 150 μm. **d**, Immunoblot showing the expression of the cited proteins or histone marks in tumor xenografts corresponding to the cited treatment groups. Tubulin and total H3 levels were used to normalize loading. A representative example of two independent experiments including three independent samples from each group of mice is shown. Full uncropped blots are available as.

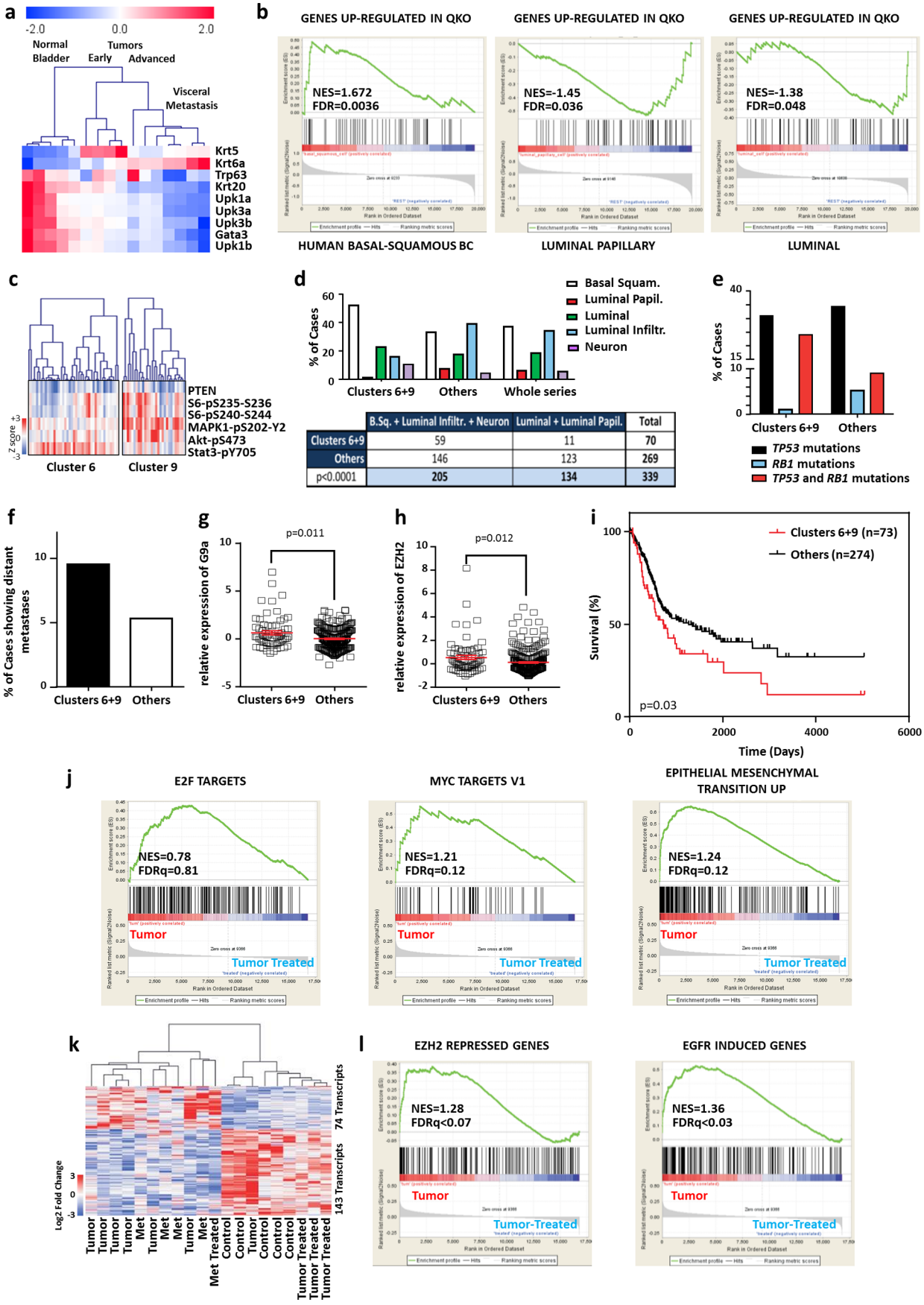

Extended Data Fig. 5 | see figure caption on next page.

Extended Data Fig. 5 | Genomic characterization of *Pten*$^{loxP/loxP}$, *Trp53*$^{loxP/loxP}$, *Rb1*$^{loxP/loxP}$and *Rbl1*$^{-/-}$ mice. a, Heatmap of normal bladder, tumors at early and advanced stages and visceral metastasis showing the expression of various genes associated with basal and luminal human BC molecular subtypes. **b**, GSEA data show the positive correlation of genes upregulated in QKO mouse tumors with upregulated genes in the human basal/squamous molecular subtype from the TCGA database, and the negative correlation of mouse upregulated genes with those upregulated in human luminal-papillary and luminal molecular subtypes. $n=5$ mouse samples. **c**, Heatmap showing the augmented activity of PKB/Akt, ERK and S6K, together with reduced PTEN expression in specific groups of human tumors (clusters 6 and 9 according to self-organizing tree algorithm (SOTA)). **d**, Clusters 6 and 9 of human tumors are enriched in basal/squamous, luminal-infiltrated and neuronal subtypes. The *P* value was obtained using a two-sided Fisher exact test. **e**, Human tumors included in clusters 6 and 9 display predominant co-occurring mutations in *RB1* and *TP53* tumor suppressor genes. **f**, Human tumors included in clusters 6 and 9 display increased distant metastasis. **g**,**h**, Human tumors included in clusters 6 and 9 display increased expression of the *G9a* (**g**) and *EZH2* (**h**) genes. Data are represented as the mean ± s.e.m. The *P* value was obtained using a two-sided Mann–Whitney *U*-test. $n=339$ patients. **i**, Kaplan–Meyer graph showing that human patients harboring tumors included in clusters 6 and 9 display decreased survival. The *P* value was obtained by log-rank test. **j**, GSEA between bladder tumors from the transgenic mouse model and tumors treated with a combination of CM-272 and CDDP, showing reduced enrichment of the *E2F* and *MYC* target genes and in genes involved in epithelial–mesenchymal transition in treated tumors. $n=5$ mouse samples. **k**, Unsupervised heatmap using the previously identified differentially expressed transcripts between tumors and normal bladder. **l**, GSEA between tumors from the transgenic mouse model (Tumor) and tumors treated with a combination of CM-272 and CDDP show increased expression in treated tumors of genes repressed by *EZH2* and decreased expression in treated tumors of genes induced by epidermal growth factor receptor in mice BC tumors. $n=5$ mouse samples.

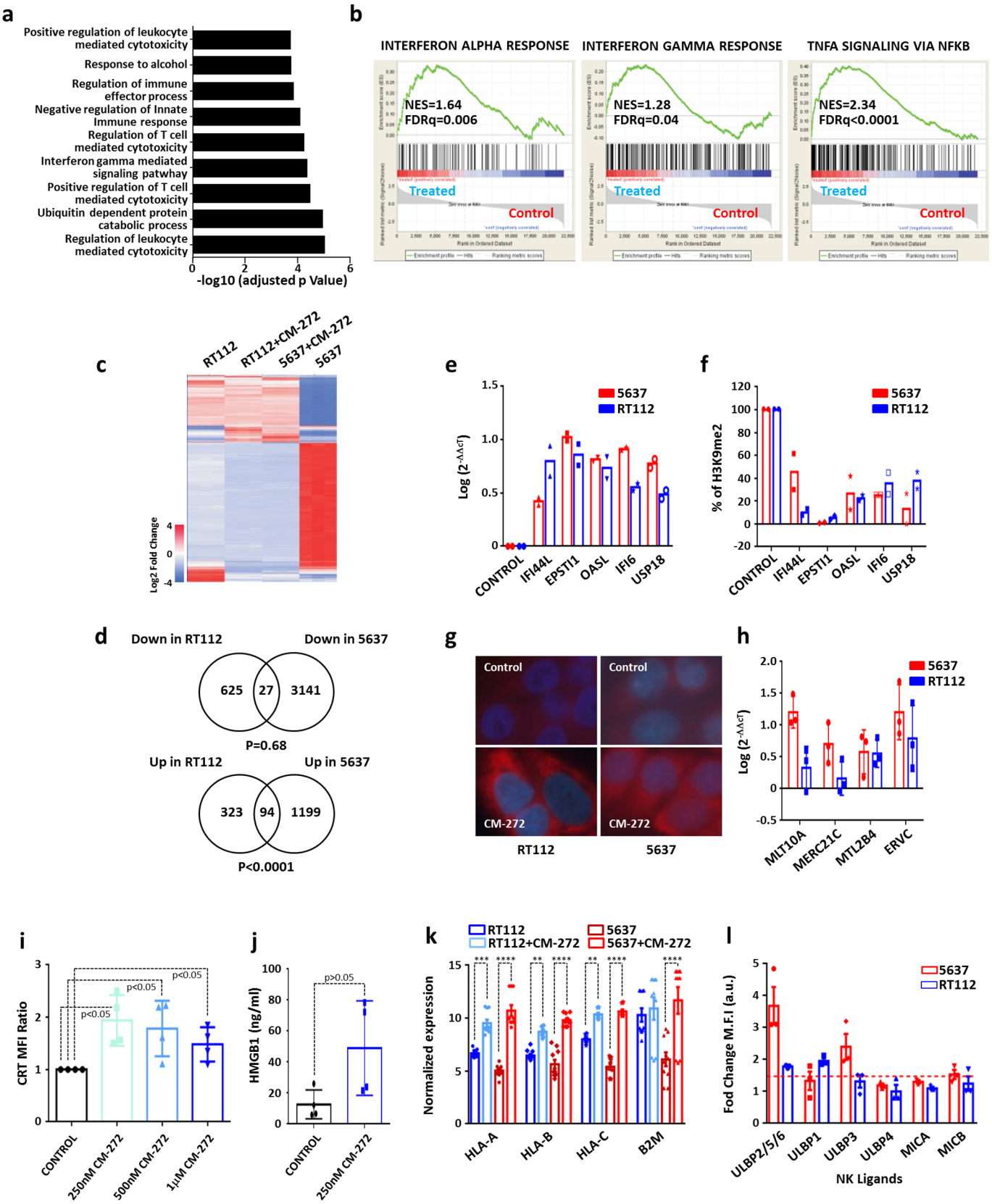

Extended Data Fig. 6 | see figure caption on next page.

Extended Data Fig. 6 | CM-272 induces an immune-mediated antitumor effect in vitro in BC. a, Gene Ontology categories upregulated in RT112 and 5637 cells after treatment with CM-272. A two-sided *t*-test was used. $n = 6$ samples. **b**, GSEA of 5637 cells treated with CM-272 versus untreated cells (Control) showing enrichment in the genes corresponding to interferon-α, interferon-γ and tumor necrosis factor-α via nuclear factor kappa-light-chain-enhancer of activated B cells response. A two-sided *t*-test was used. $n = 6$ samples. **c**, Heatmap showing gene expression changes in RT112 and 5637 BC cell lines after CM-272 treatment. **d**, Venn diagrams showing the overlapping transcripts down- (upper panel) or upregulated (lower panel) by CM-272 treatment in the RT112 and 5637 BC cell lines. A one-sided Fisher's exact test was used. **e**, RT-qPCR of interferon-response genes in RT112 and 5637 cell lines after treatment with CM-272 for 48 h. $n = 2$ independent experiments. The data represent the mean value. **f**, ChIP with qPCR analysis of interferon-response genes in RT112 and 5637 cells treated for 48 h (700 and 880 nM, respectively). $n = 2$ independent experiments. The data represent the mean value. **g**, Immunofluorescence of dsRNAs after treatment of 5637 and RT112 cells with CM-272. A representative example of three independent experiments is shown. **h**, RT-qPCR analysis of endogenous retroviruses after treatment of 5637 and RT112 cells with CM-272. $n = 3$ independent experiments. The data represent the mean ± s.d. **i**, Calreticulin exposure determined by flow cytometry in RT112 cells after 48 h of treatment with 250, 500 and 1000 nM of CM-272. MFI ratio of calreticulin expression: MFI ratio of calreticulin expression $= \frac{\text{MFI for calreticulin after CM} - 272 \text{ treatment}}{\text{MFI for calreticulin of untreated cells}}$. $n = 4$ independent experiments. The data represent the mean ± s.d. The *P* value was estimated using a two-tailed Mann–Whitney *U*-test. $^*P < 0.05$. **j**, HMBG1 secretion determined by ELISA analysis in the supernatants of RT112 cells after treatment with CM-272 for 48 h. n = 4 independent experiments. The data represent the mean ± s.d. The *P* value was estimated using a two-tailed Mann–Whitney *U*-test. $^*P < 0.05$. **k**, Expression of major histocompatibility genes in the RT112 and 5367 cell lines before and after treatment with CM-272. The data represent the mean ± s.e.m. The *P* value was obtained using a one-sided Mann–Whitney *U*-test. $n = 3$ samples. **l**, Expression of cited natural killer cell ligands in RT112 and 5637 cells after treatment with CM-272 for 48 h. The data represent the mean ± s.e.m. $n = 6$ samples.

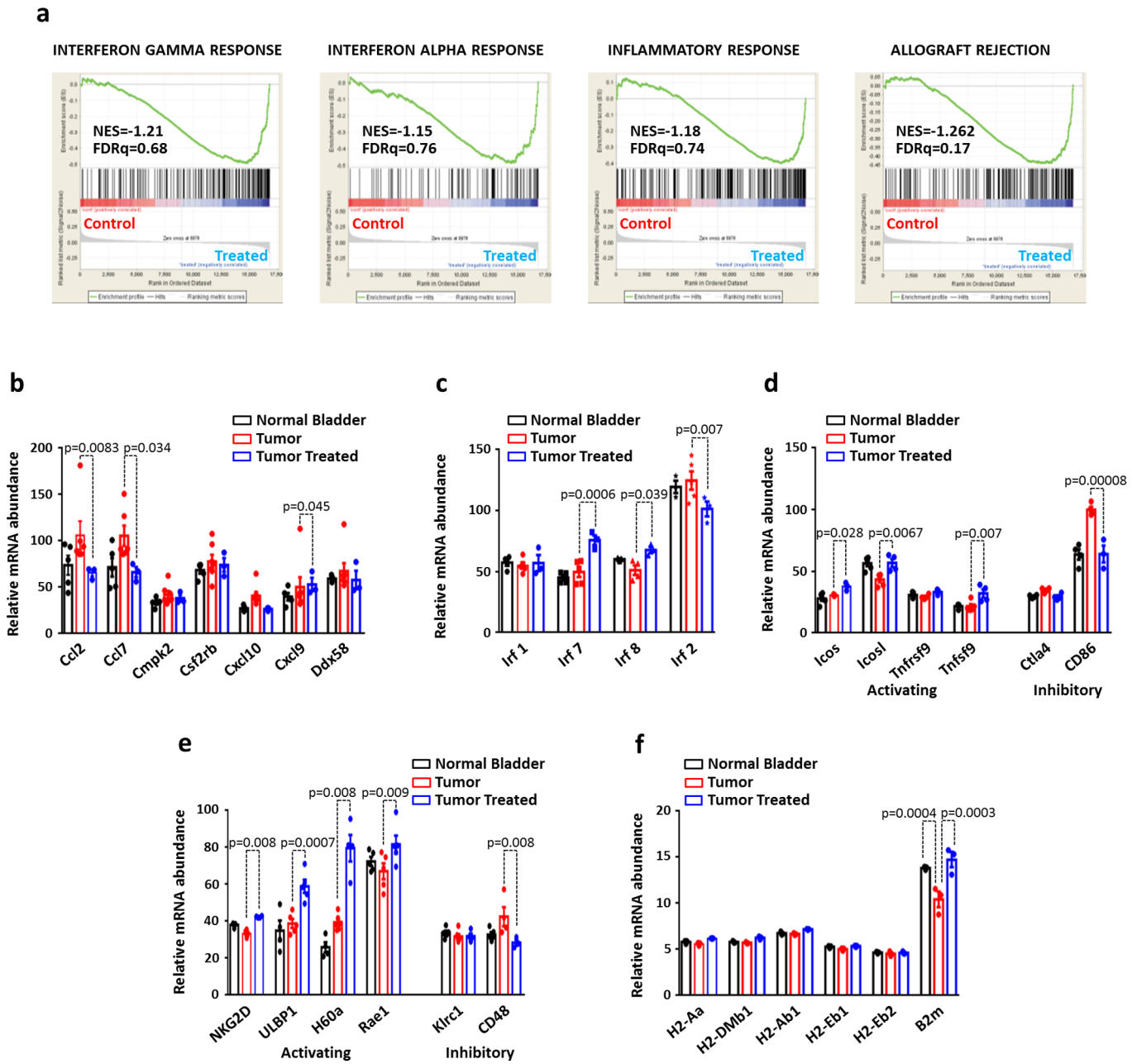

Extended Data Fig. 7 | CM-272 induces an immune-mediated antitumor effect in vivo in BC. a, GSEA between normal bladder (Control) and CM-272 + CDDP-treated BC tumors from the transgenic mouse model showing enrichment in the genes corresponding to interferon-γ, interferon-α, inflammatory response and allograft rejection in the treated tumors. $n = 4$ samples. **b**, Expression of negative immunoregulatory cytokines and chemoattractants in BC tumors from transgenic mice treated with CM-272 + CDDP. The *P* value was obtained using a one-sided Mann–Whitney *U*-test. $n = 3$. **c**, Expression of interferon regulatory factors in BC tumors from animals treated with CM-272 and CDDP. *P* value was obtained using a one-sided Mann–Whitney *U*-test. $n = 3$. **d**, Expression of T cell activators in BC tumors from animals treated with CM-272 and CDDP. *P* value was obtained using a one-sided Mann–Whitney *U*-test. $n = 3$. **e**, Expression of NKG2D ligands and receptors in BC tumors from animals treated with CM-272 + CDDP. The *P* value was obtained using a one-sided Mann–Whitney *U*-test. $n = 3$. **b**–**e**, Results are shown as the mean ± s.e.m. of three independent experiments. **f**, Expression of major histocompatibility genes in BC tumors from animals treated with CM-272 + CDDP. The data represent the mean ± s.e.m. The *P* value was obtained using a one-sided Mann–Whitney *U*-test. $n = 3$.

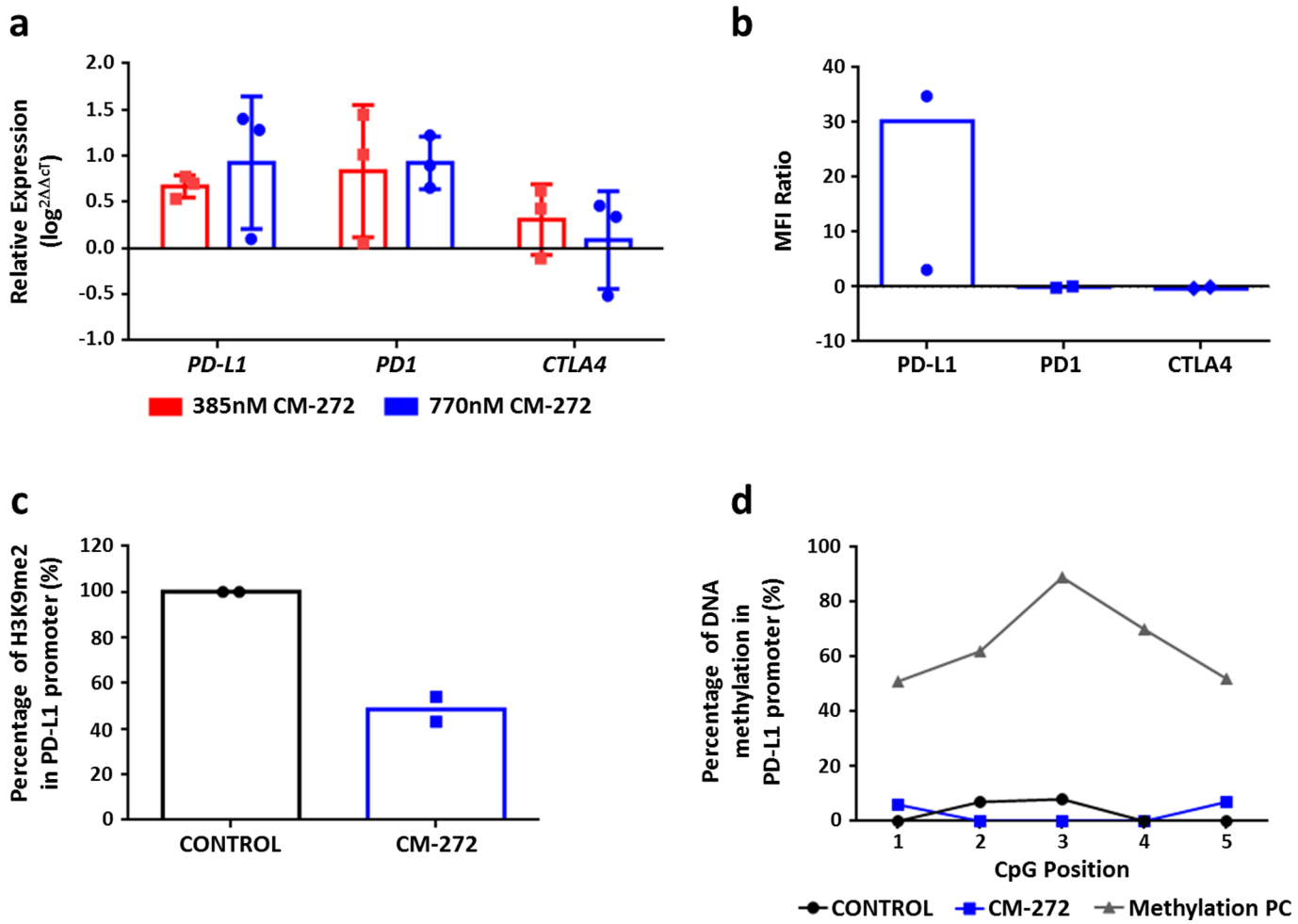

Extended Data Fig. 8 | Expression and epigenetic regulation analysis of *PD-L1*, *PD-1* and *CTLA4* in the RT112 cell line. a, RT-qPCR analysis of *PD-L1*, *PD-1* and *CTLA4* in the RT112 cell line after treatment with CM-272 for 48 h. $n = 3$ independent experiments. The data represent the mean with regard to untreated cells. **b**, Flow cytometry analysis of PD-L1, PD1 and CTLA4 levels after treatment with CM-272 for 48 h. The MFI ratio is represented as: $\text{MFI ratio} = \frac{(\text{MFI for immune checkpoint/MFI for isotype control after CM} - 272\ \text{treatment})}{(\text{MFI for immune checkpoint/MFI for isotype control of untreated cells})}$. $n = 2$ independent experiments. **c**, Quantitative ChIP–PCR analysis of H3K9me2 levels in the *PD-L1* promoter region in the RT112 cell line after treatment with CM-272 for 48 h. $n = 2$ independent experiments. **d**, DNA methylation analysis by pyrosequencing of the promoter region of *PD-L1* after CM-272 treatment. The data shown are representative of two independent experiments. Control: untreated RT112 cells; CM-272: RT112 cells after CM-272 treatment; Methylation-positive control: methylation-positive control is a universally methylated DNA.

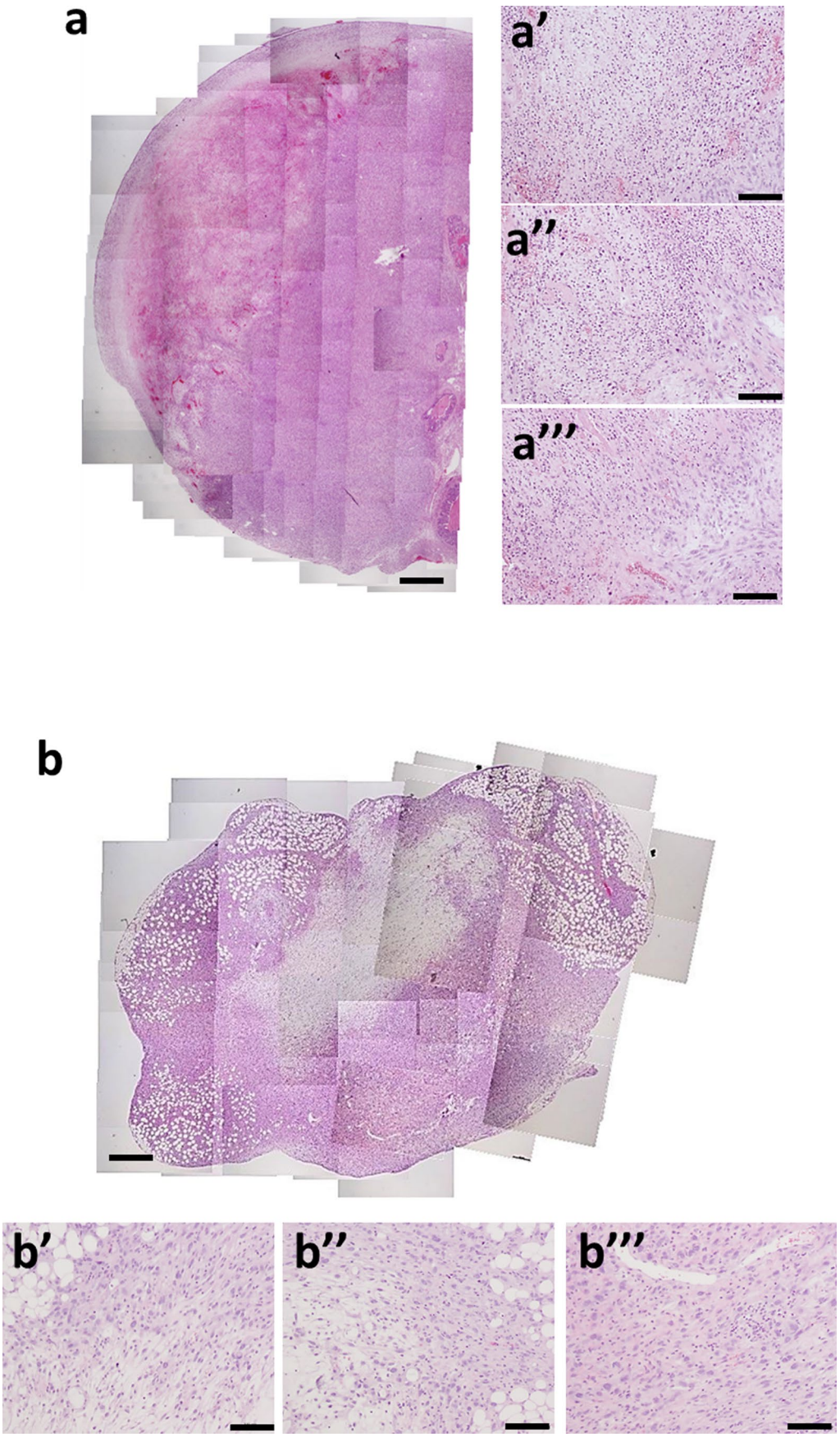

Extended Data Fig. 9 | see figure caption on next page.

Extended Data Fig. 9 | Appearance of a tumor and a metastasis in QKO mice. a, Histological appearance of a tumor 1 month after the end of treatment with CM-272 and anti-PD-L1. a′, a′′ and a′′′ show three areas of **a** at high magnification. A representative example of three independent lesions is shown. **b**, Histological appearance of a metastatic lesion 1 month after the end of treatment with CM-272 and anti-PD-L1. b′, b′′ and b′′′ show three areas of **b** at high magnification. Note the presence of necrotic and highly inflamed areas close to those showing normal tumor cell appearance. **a**,**b**, scale bar, 1 mm; a′, a′′, a′′ and b′, b′′, b′′, scale bar, 200 μm. A representative example of three independent lesions is shown.

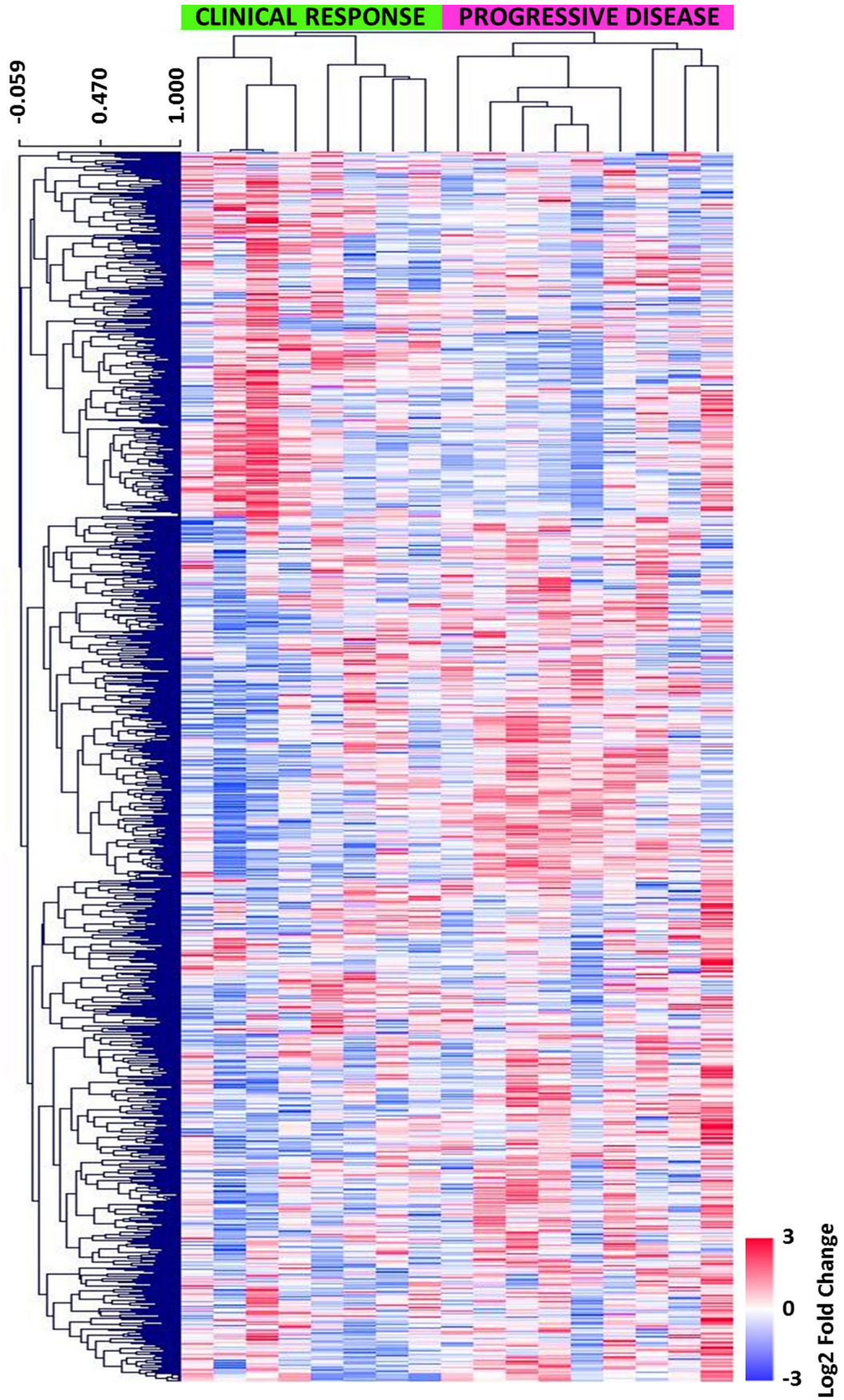

Extended Data Fig. 10 | Increased expression of *G9a* and *EZH2* in non-responders treated with anti-PD-1 immunotherapy. Heatmap showing the supervised classification of genes bound by *G9* and *EZH2* in advanced urothelial carcinoma patients that responded or progressed to PD-1 treatment.

nature research

Corresponding author(s): *Double-blind peer review submissions: write DBPR and your manuscript number here instead of author names.*

Last updated by author(s): *YYYY-MM-DD*

Reporting Summary

Nature Research wishes to improve the reproducibility of the work that we publish. This form provides structure for consistency and transparency in reporting. For further information on Nature Research policies, see Authors & Referees and the Editorial Policy Checklist.

Statistics

For all statistical analyses, confirm that the following items are present in the figure legend, table legend, main text, or Methods section.

n/a	Confirmed	
☐	☒	The exact sample size (*n*) for each experimental group/condition, given as a discrete number and unit of measurement
☐	☒	A statement on whether measurements were taken from distinct samples or whether the same sample was measured repeatedly
☐	☒	The statistical test(s) used AND whether they are one- or two-sided *Only common tests should be described solely by name; describe more complex techniques in the Methods section.*
☐	☒	A description of all covariates tested
☐	☒	A description of any assumptions or corrections, such as tests of normality and adjustment for multiple comparisons
☐	☒	A full description of the statistical parameters including central tendency (e.g. means) or other basic estimates (e.g. regression coefficient) AND variation (e.g. standard deviation) or associated estimates of uncertainty (e.g. confidence intervals)
☐	☒	For null hypothesis testing, the test statistic (e.g. *F*, *t*, *r*) with confidence intervals, effect sizes, degrees of freedom and *P* value noted *Give P values as exact values whenever suitable.*
☒	☐	For Bayesian analysis, information on the choice of priors and Markov chain Monte Carlo settings
☐	☒	For hierarchical and complex designs, identification of the appropriate level for tests and full reporting of outcomes
☐	☒	Estimates of effect sizes (e.g. Cohen's *d*, Pearson's *r*), indicating how they were calculated

Our web collection on statistics for biologists contains articles on many of the points above.

Software and code

Policy information about availability of computer code

Data collection	Transcriptomic data have been deposited in GEO GSE115544, GSE115485, and GSE111636
Data analysis	The commercial software used for data analysis is properly described in the SUPP. INFO. Multiexperiment viewer 4.9.0; Transcriptome array console 4.0 (Applied Biosystems); Gene Set Enrichment Analyses 3.0 (Broad Institute and UC San Diego), Enrich webtool (http://amp.pharm.mssm.edu/Enrichr/) ; IBM SPSS 20.0, GraphPad prism 6.0; Calcusyn software, Biosoft 2.1; CellQuest™ software (BD Biosciences) 5.1; PyroQ-CpG analysis software 1.0.9; ImageLab 6.0.1 BioRad.

For manuscripts utilizing custom algorithms or software that are central to the research but not yet described in published literature, software must be made available to editors/reviewers. We strongly encourage code deposition in a community repository (e.g. GitHub). See the Nature Research guidelines for submitting code & software for further information.

Data

Policy information about availability of data

All manuscripts must include a data availability statement. This statement should provide the following information, where applicable:

- Accession codes, unique identifiers, or web links for publicly available datasets
- A list of figures that have associated raw data
- A description of any restrictions on data availability

Microarray data are deposited in GEO with accesion numbers GSE115544, GSE115485, and GSE111636. These data will be freely accesible once the manuscript is published

Field-specific reporting

Please select the one below that is the best fit for your research. If you are not sure, read the appropriate sections before making your selection.

☒ Life sciences ☐ Behavioural & social sciences ☐ Ecological, evolutionary & environmental sciences

For a reference copy of the document with all sections, see nature.com/documents/nr-reporting-summary-flat.pdf

Life sciences study design

All studies must disclose on these points even when the disclosure is negative.

Sample size	No sample size was calculated. All availble samples were included in each analysis.
Data exclusions	No data were excluded. Only those samples with no available material or enough quality (ie. poor quality or no FFPE sections) were excluded from the analyses
Replication	All experiments and measures were made at least in triplicate (specific replicates are given for each particular experiment) obtaining in all of the cases the similar results. For immunoblots in general duplicate independent blots were performed with similar results. In specific experiments (immunoblots from transgenic mouse samples and duplicate of different samples were included in the same membrane.
Randomization	Patient data have been randomized or classified accoridng clinical covariates. All experiments made in mice assigned the different groups randomly (i.e.: treated or untreated)
Blinding	Investigator were blinded to group allocation during diverse analyses using clinical or mouse samples

Reporting for specific materials, systems and methods

We require information from authors about some types of materials, experimental systems and methods used in many studies. Here, indicate whether each material, system or method listed is relevant to your study. If you are not sure if a list item applies to your research, read the appropriate section before selecting a response.

Materials & experimental systems

n/a	Involved in the study
☐	☒ Antibodies
☐	☒ Eukaryotic cell lines
☒	☐ Palaeontology
☐	☒ Animals and other organisms
☐	☒ Human research participants
☐	☒ Clinical data

Methods

n/a	Involved in the study
☒	☐ ChIP-seq
☐	☒ Flow cytometry
☒	☐ MRI-based neuroimaging

Antibodies

Antibodies used	All antibodies were from commercial sources and are properly descibed in Suppl. Info. For immunoblots: antibodies used against G9a (abcam ab180815), EZH2 (Abnova MAB9542) , H3K9me2 (Abcam ab1220), H3K27me3 (Millipore 07-449), H3K9me3(Abcam ab8898), AKT-P (Ser473) (Cell Signaling cs-4060), Cleaved Caspase-3 Asp175 (Cell Signaling 9661S, cleaved PARP (BD 611039), LC3B (Abcam ab48394) that predict the forms LCI/ LCII, Rb total (BD Pharmigen 554136), p53 (Novocastra NCl-p53_CM5p), PTEN (Santa Cruz SC 6818), ERK total (Santa Cruz SC-94), ERK1/2-P (Thr202/Tyr204) (Cell Signaling 4370), Akt1/2 (Santa Cruz SC 1619), Stat3 (Cell Signaling 4904), Stat3-P (Tyr705) (Cell Signaling 9131), ribosomal S6 (Cell Signaling cs-2317), and S6-P (Ser 235/236) (Cell Signaling cs-2211). Loading was controlled by using anti-GAPDH (Santa Cruz sc-25778) or anti- β-actin (Santa Cruz sc-1616) antibodies. For Dot Blot, Monoclonal antibody 5-Methylcytidine, Cat No BI-MECY-1000, Eurogentec, diluted 1:4000 . For Immunofluorescence (dsRNA detection) monoclonal antibody J2 (10010200, Scicons), dilution 1:150. For immunohistochemistry in addition to those mentioned in the immunoblot CD163 (Abcam ab74604), CD8 (Abcam ab 203035), NK1.1 (553164 BD Pharmingen) Flow cytometry for NKG2D ligands: MICA-PE (159227), MICB-PE (236511), ULBP1-PE (170818), ULBP3-PE (166510), ULBP4-PE (709116) and ULBP2/5/6-PE (165903 RyD systems, Mineapolis, MN)
Validation	The antibodies employed in our study were validated by the manufacturers and used according to the manufacturers' instructions.

Eukaryotic cell lines

Policy information about cell lines

Cell line source(s)	All cell lienes used were generously donated by Dr. FX Real (CNIO, Madrid, Spain). The full description of these cell lines is reported in Earl, J., et al. The UBC-40 Urothelial Bladder Cancer cell line index: a genomic resource for functional studies. BMC Genomics 16, 403 (2015).
Authentication	STR validation at the lab of origin, cells were grown for no more than 15 passages upon thawing
Mycoplasma contamination	Tested routinely every two weeks by PCR and immediately after cell thawing. All experiments were carried out in negative cultures.
Commonly misidentified lines (See ICLAC register)	None of the cell lines used is reported at ICLAC register

Animals and other organisms

Policy information about studies involving animals; ARRIVE guidelines recommended for reporting animal research

Laboratory animals	For xenograft experiments eight-week-old female NMRI-FoxN1nu/nu mice (Janvier Saint-Berthevin, France) were used. The trasgenic mice were under mixed background and the Rb1F/F; Tp53F/F ; PtenF/F ;Rbl1-/-mice were generated by breeding Rb1F/F; Rbl1-/- and Tp53F/F ;PtenF/F mice, reported in Costa, C., et al. A novel tumor suppressor network in squamous malignancies. Scientific reports 2, 828 (2012) and Moral, M., et al. Akt activation synergizes with Tp53 loss in oral epithelium to produce a novel mouse model for head and neck squamous cell carcinoma. Cancer Res 69, 1099-1108 (2009), respectively
Wild animals	The study does not involve wild animals
Field-collected samples	The study does not involve samples collected from the field
Ethics oversight	nude mice, approved by the Animal Welfare Department of the Comunidad de Madrid (ProEX 183/15). Transgenic mouse model and related methods and experiments were approved by the Animal Ethical Committee and conducted in compliance with Centro de Investigaciones Energéticas, Medioambientales y Tecnológicas (CIEMAT) guidelines. The specific procedures have been approved by Comunidad Autónoma de Madrid (ProEX 088/15)

Note that full information on the approval of the study protocol must also be provided in the manuscript.

Human research participants

Policy information about studies involving human research participants

Population characteristics	Tumor samples and medical records were analyzed from 87 bladder cancer patient cohort Hospital "12 de Octubre" previously reported 1. Samples and united data from patients included in this study were provided by the Biobanco i+12 in the Hospital "12 de Octubre" integrated in the Spanish Hospital Biobanks Network (RetBioH; www.redbiobancos.es) following standard operation procedures with appropriate approval of the RETHICAL AN Scientific Committees. Metastatic urothelial carcinoma samples were obtained from primary lesions of 17 patients before undergoing therapy with pembrolizumab. All patients provided written consent prior to any eligibility procedures and were enrolled in the study. All subjects received pembrolizumab 200 mg every three weeks until disease progression or until completion of 2 years of therapy regardless of PD-L1 status. Formalin-fixed paraffin-embedded (FFPE) tumor specimens with sufficient viable tumor content were required prior to the start of study treatment. Specific population demographics and clinical data are provided in Supplementary Information of the manuscript
Recruitment	No bias was generated during clinical assesment. Al NMIBC patients were included without selection. The criteria for pembrolizumab treatment are reported in the trial KEYNOTE-052, NCT02335424. Only patients treated at Hosp Univ 12 de Octubre were included. For RTU specimens no specific criteria was used. For anti PD-1 therapy, the samples correspond to trial NCT02335424. All patients provided written consent prior to any eligibility procedures and were enrolled in the study if they met the following inclusion and exclusion criteria: had histologically or cytologically documented locally advanced unresectable (T4b, any N; or any T, N 2–3) or metastatic (M1, Stage IV) UC (including renal pelvis, ureter, urinary bladder and urethra), had not received prior systemic chemotherapy (i.e., first-line therapy) and were not eligible to receive cisplatin; had confirmed measurable disease defined by Response Evaluation Criteria in Solid Tumors version 1.1 (RECIST v1.1); adequate hematologic and end-organ function; and no autoimmune disease or active infection. Patients were considered cisplatin-ineligible if they met at least one of the following criteria: a. Eastern Cooperative Oncology Group (ECOG) performance status of 2 b. creatinine clearance < 60mL/min but ≥30mL/min c. Common Terminology Criteria for Adverse Events (CTCAE) v.4 Grade ≥2 audiometric hearing loss d. CTCAE v.4 Grade ≥2 peripheral neuropathy or e. New York Heart Association (NYHA) class III heart failure. Patients could have undergone prior therapies for their local disease including surgery and bacillus Calmette–Guerin (BCG) vaccine. All subjects received pembrolizumab 200 mg every three weeks until disease progression or until completion of 2 years of therapy regardless of PD-L1 status. Formalin-fixed paraffin-embedded (FFPE) tumor specimens with sufficient viable tumor content were required prior to the start of study treatment. .
Ethics oversight	Tumor samples and medical records were analyzed from 87 bladder cancer patient cohort Hospital "12 de Octubre" previously reported1. Samples and united data from patients included in this study were provided by the Biobanco i+12 in the Hospital "12

de Octubre" integrated in the Spanish Hospital Biobanks Network (RetBioH; www.redbiobancos.es) following standard operation procedures with appropriate approval of the RETHICAL AN Scientific Committees. Metastatic urothelial carcinoma samples were obtained from primary lesions of 17patients before undergoing therapy with pembrolizumab. All patients provided written consent prior to any eligibility procedures and were enrolled in the study.

Note that full information on the approval of the study protocol must also be provided in the manuscript.

Clinical data

Policy information about clinical studies

All manuscripts should comply with the ICMJE guidelines for publication of clinical research and a completed CONSORT checklist must be included with all submissions.

Clinical trial registration	No specific clinical trial directly related with this study is included. All NMIBC patients were included without selection. The criteria for pembrolizumab treatment are reported in the trial KEYNOTE-052, NCT02335424. Only patients treated at Hospital University 12 de Octubre were included.
Study protocol	For anti PD-1 therapy, the samples correspond to trial NCT02335424. All patients provided written consent prior to any eligibility procedures and were enrolled in the study if they met the following inclusion and exclusion criteria: had histologically or cytologically documented locally advanced unresectable (T4b, any N; or any T, N 2–3) or metastatic (M1, Stage IV) UC (including renal pelvis, ureter, urinary bladder and urethra), had not received prior systemic chemotherapy (i.e., first-line therapy) and were not eligible to receive cisplatin; had confirmed measurable disease defined by Response Evaluation Criteria in Solid Tumors version 1.1 (RECIST v1.1); adequate hematologic and end-organ function; and no autoimmune disease or active infection. Patients were considered cisplatin-ineligible if they met at least one of the following criteria: a. Eastern Cooperative Oncology Group (ECOG) performance status of 2 b. creatinine clearance < 60mL/min but ≥30mL/min c. Common Terminology Criteria for Adverse Events (CTCAE) v.4 Grade ≥2 audiometric hearing loss d. CTCAE v.4 Grade ≥2 peripheral neuropathy or e. New York Heart Association (NYHA) class III heart failure. Patients could have undergone prior therapies for their local disease including surgery and bacillus Calmette–Guerin (BCG) vaccine. All subjects received pembrolizumab 200 mg every three weeks until disease progression or until completion of 2 years of therapy regardless of PD-L1 status. Formalin-fixed paraffin-embedded (FFPE) tumor specimens with sufficient viable tumor content were required prior to the start of study treatment.
Data collection	Data collection and periods under study for each cohort have been previously defined in Balar et al., First-line pembrolizumab in cisplatin-ineligible patients with locally advanced and unresectable or metastatic urothelial cancer (KEYNOTE-052): a multicentre, single-arm, phase 2 study Lancet Oncol. 2017 Nov;18(11):1483-1492 and Dueñas et al., PIK3CA gene alterations in bladder cancer are frequent and associate with reduced recurrence in non-muscle invasive tumors. Mol Carcinog. 2015 Jul;54(7):566-76.
Outcomes	The evolution and response of any measurable disease were as defined by Response Evaluation Criteria in Solid Tumors version 1.1 (RECIST v1.1). For the NMIBC cohort recurrence was defined as the appearance of new tumor lesion in the bladder of a patient that has undergone RTU for a previous lesion. Progression was defined as the appearance of higher histological stage or grade in recurrent tumors.

Flow Cytometry

Plots

Confirm that:

☒ The axis labels state the marker and fluorochrome used (e.g. CD4-FITC).

☒ The axis scales are clearly visible. Include numbers along axes only for bottom left plot of group (a 'group' is an analysis of identical markers).

☐ All plots are contour plots with outliers or pseudocolor plots.

☒ A numerical value for number of cells or percentage (with statistics) is provided.

Methodology

Sample preparation	For cell cycle analysis, 250.000 cells were treated for 24 and 48 hours with GI50 concentration of CM-272 (700nM for RT112 and 880nM for 5637 cells). Then, cells were washed twice with phosphate-buffered saline (PBS) and resuspended in 0.2 % Tween-20 in PBS and 0.5 mg/mL Rnase A (Ribonuclease A Type III-A from bovine pancreas, Cat No R5125, Sigma) and incubated for 30 min at 37 °C. Subsequently, cells were stained with 25 µg/mL of propidium iodide (Cat No P4170, Sigma). For apoptosis assay, 100.000 cells were treated for 24 hours with CM-272 at different concentrations (GI25, GI50 and GI75). The FITC Annexin V Apoptosis Detection Kit I (Cat. No. 556419, BD Pharmingen) was used following the manufacturer's instructions, with some modification. Firstly, cells were washed twice with PBS and resuspended in 1X Binding Buffer at a concentration of 1x106 cells/mL. 1 µL of FITC Annexin V (AV) antibody and 2 µL of propidium iodide (PI) were added and incubated for 15 min at RT in the dark. Finally, 400 µL of 1X Binding Buffer were added to each tube and analyzed by flow cytometry within 1 h. We represented the addition of FITC AV positive and PI negative cells (early apoptosis) and FITC AV positive and PI positive cells (end stage apoptosis, death). For calreticulin exposure, cells were harvested and washed with ice-cold PBS, then incubated with a CRT-specific antibody (Abcam) diluted in cold blocking buffer (5 % BSA in PBS) for 30 min on ice, washed, and incubated with an FITC-conjugated antibody (Sigma) in blocking buffer for 30 min. Thereafter, cells were washed, stained with 1 µg/mL TO-PRO-3 (Life Technologies) in cold PBS for 5 min. For NKG2D ligands, cells were detached with trypsin and washed in PBS/BSA. Then, 1x10(5) cells were labeled with the follow monoclonal antibodies for NKG2D ligands: MICA-PE (159227), MICB-PE (236511), ULBP1-PE (170818), ULBP3-PE (166510), ULBP4-PE (709116) and ULBP2/5/6-PE (165903 RyD systems, Mineapolis, MN). After 30 minutes at 4ºc cells were washed and

	resuspended in PBS/PBA with DAPI to discard dead cells in the flow cytometry analysis. The fold change of mean fluorescence intensity (MFI) for each NKG2D ligand was evaluated regarding its corresponding level in the no treated culture performed in parallel.
Instrument	BD FACSCalibur flow cytometer (Becton Dickinson, San Jose, CA, USA)
Software	FLOWJO
Cell population abundance	Not applicable
Gating strategy	Not applicable

☐ Tick this box to confirm that a figure exemplifying the gating strategy is provided in the Supplementary Information.